Molecular Therapy
Nucleic Acids
Original Article

# The AT Interstrand Cross-Link: Structure, Electronic Properties, and Influence on Charge Transfer in dsDNA

Boleslaw T. Karwowski[1]

[1]DNA Damage Laboratory of Food Science Department, Faculty of Pharmacy, Medical University of Lodz, ul. Muszynskiego 1, 90-151 Lodz, Poland

**The interaction of chemical and physical agents with genetic material can lead to almost 80 different DNA damage formations. The targeted intentional DNA damage by radiotherapy or chemotherapy is a front-line anticancer therapy. An interstrand cross-link can result from ionization radiation or specific chemical agents, such as trans-/cisplatin activity. Here, the influence of the adenine and thymidine (AT) interstrand linkage, the covalent bond between the adenine N6 and thymidine C5 methylene group, on the isolated base pair as well as double-stranded DNA (dsDNA) was taken into quantum mechanical/molecular mechanical (QM/MM) consideration at the m062x/6-31+G*:UFF level of theory in the aqueous phase. All the results presented in this article, for the first time, show that an AT-interstrand cross-link (ICL) changes the positive and negative charge migration process due to a higher activation energy forced by the cross-link's presence. However, the final radical cation destination in cross-linked DNA is left in the same place as in a native double-stranded-deoxyoligonucleotide. Additionally, the direction of the radical anion transfer was found to be opposite to that of native dsDNA. Therefore, it can be postulated that the appearance of the AT-ICL does not disturb the hole migration in the double helix, with subsequent effective changes in the electron migration process.**

## INTRODUCTION

Genetic information, which is the seed of life located in a cell nucleus, is continuously exposed to ionization radiation or other harmful or mutation environmental conditions. The interaction of physical or chemical agents with DNA can lead to different kinds of lesions, e.g., base modification, single or double-strand break, tandem lesion, inter- and intrastrand cross-link, apurinic/apirimidinic (AP) site, etc.[1] The formed modification can trigger a mutation in genetic information or can lead to serious consequences in the replication or transcription processes.[2,3] Until now, almost 80 types of DNA damage are known, most of which are repaired from the genome by base (BER) or nucleotide (NER) excision repair systems.[4,5] However, the interstrand cross-link (ICL), which is one of the most serious DNA lesions, is removed by the complicated process of homologous recombination (HR) or non-homologous end joining (NHEJ) systems.[6] It has been assumed that the appearance of 40 ICL events on a bacterial genome is lethal for a cell.[7]

The above-mentioned DNA damage can be the result of chemical and/or physical agent activities. Due to the difference in nature of the initial factors, it can be expected that the structures of the formed ICL should be different. The interaction of chemical cross-link agents, such as psoralen, mitomicyn, iperits, cis-/transplatin, etc., with a double-stranded oligonucleotide can lead to different types of complementary oligonucleotide strands bridging (Figure 1).[6,8] The evoked adduct can change significantly the spatial structure of double-stranded DNA (dsDNA), brought about by incorporating part of or the whole of the ICL agent. Due to the high toxicity of the ICL cell, the molecules that lead to their formation in the genome have been of interest in chemotherapy since 1946.[9] However, this front-line anticancer therapy came as a result of the use of the horrific Second World War weapon sulfur mustard (commonly known as mustard gas).[9]

It is important to mention here that chemical and physical agents that cause DNA ICLs induce a variety of other DNA damage types alongside. Nitrogen mustard and cisplatin induce around 5% of ICLs.[10] In the case of cisplatin therapy, the intrastrand cross-link has been identified as the main result.[11] Also, a high-fat diet, alcoholism, and smoking can be perceived as suitable sources of lipid peroxidation products (acrolein and aldehydes), which can cause DNA interstrand cross-linking.[12–16] The situation is opposite in the case of physical factors, such as ionization radiation, due to the fact that none of the additional molecules is inserted into the dsDNA structure. Therefore, the double-helix structure should be appropriately reorganized with minimum spatial distortion and energy requirements.

Both types of radiation, different in energy (low and high LET [linear energy transfer]) cause the appearance of ICLs within the genome in two ways.[17,18] On the one hand, an ICL is an indirect product of radiation, i.e., an ICL as a reaction product of the AP sites' aldehyde group (initially formed) with an exocyclic amino group of

Received 1 May 2018; accepted 22 October 2018;
https://doi.org/10.1016/j.omtn.2018.10.014.

**Correspondence:** Boleslaw T. Karwowski, DNA Damage Laboratory of Food Science Department, Faculty of Pharmacy, Medical University of Lodz, ul. Muszynskiego 1, 90-151 Lodz, Poland.
**E-mail:** bolek.karwowski@wp.pl

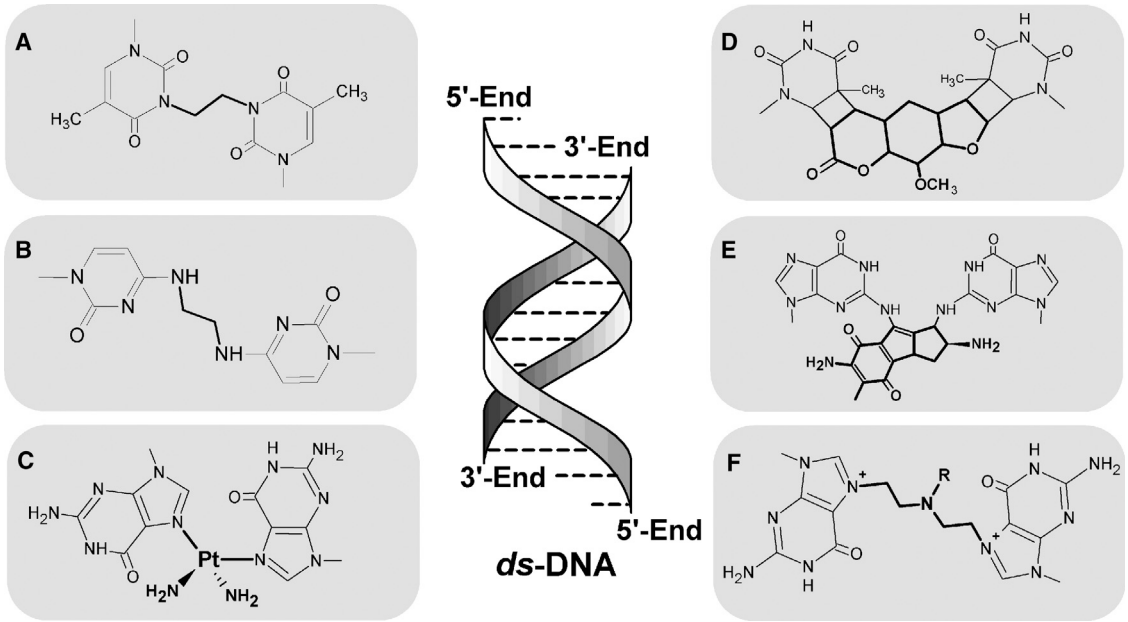


**Figure 1. DNA Interstrand Cross-Link**

(A–F) DNA interstrand cross-link was forced by the following chemical agents: (A) $N^3$T-Ethyl-$N^3$T-ICL, (B) $N^4$C-Ethyl-$N^4$C-ICL, (C) *cis-/trans*platin, (D) psoralen, (E) mitomicyn, and (F) iperits.[6,8]

nucleobases in the complementary strand (Figure 2A).[19] On the other hand, an ICL can be perceived as the direct result of charge transfer through dsDNA initiated by photosensitizer and UV interaction or ionization radiation, for example.[20,21] In this case, the primary yield thymine methyl radical reacts with the endocyclic amino group (N1) of adenine with a subsequent Dimroth-like rearrangement (Figure 2B).[22,23] In this article, emphasis has been put on the influence of the adenine and thymidine (AT)-ICL on the spatial geometry and electronic properties of double-stranded oligonucleotide, as well as hydrogen bond (HB) and stacking interaction energies. Moreover, the role of the AT-ICL in the dsDNA charge transfer was taken into consideration.

## RESULTS AND DISCUSSION

On account of two significant chemical limitations of direct N6-C5 interstrand AT cross-link induction by ionization radiation within double-stranded oligonucleotides, i.e., the low reaction yield of AT-ICL formation and the complication of its specific localization, a theoretical approach was used. (Recently, Hong and Greenberg[24] proposed a new phenyl selenide strategy that avoids these restrictions.) The *in silico* experiments of the influence of an AT-ICL on dsDNA spatial geometry were performed in a condensed (aqueous) phase to properly mimic the cellular environment. For this strategy, the polarizable continuum model (PCM) model was used instead of a solvent periodic box or artificial water molecules attached to each base pair.[25] It is known that, for the B form of DNA, each AT and GC pair inhered 44 and 27 $H_2O$ molecules, respectively, which formed the solvation layer.[26] This hydrated web stabilized the three-dimensional dsDNA structure, and it indirectly influenced the HB and stacking interaction energy. The complexity of the proposed system makes the quantum mechanics or density functional theory (DFT) calculation highly time consuming. To reduce the cost, quantum mechanical molecular mechanical (QM/MM) methodology was thus chosen for these studies.[27]

A brief look at the double-DNA helix revealed that its shape depends on the mutual base pair location; the strength of HBs; stacking integration; and, which is less obvious, the sugar phosphate backbone spatial arrangement.[28] The last factor plays an important role in double-helix organization, especially when, for example, in bulk lesion, intercalators are present in its structure. This external framework of double helix displays a high flexibility, which is derived from the large number of 2′-deoxyrybose freedom degrees.[29] The power of the furanose ring's adaptability is well described by pseudorotation cycle.[30] Moreover, the DNA sugar phosphate backbone, as has been shown in previous studies of phosphorothioaes and DNA-low-energy electron interactions, can influence charge transfer through double-stranded oligonucleotides.[31]

### The Structure and Electronic Properties of Isolated AT-ICLs

The discussed AT ICL is the result of charge migration through the dsDNA activated by photoexcitation of the antrachinone moiety attached to the 5′ end of one of the strands, as has been shown by Cadet and colleagues.[20] This process is initiated by the hydrogen atom loss from the thymine $CH_3$ group with a subsequent methylene radical formation. The yield of the final AT-ICL followed a thymidine-adenine C5-N3 bond formation with a subsequent Dimroth-like purine ring rearrangement (Figure 2B).[22] From a structural point

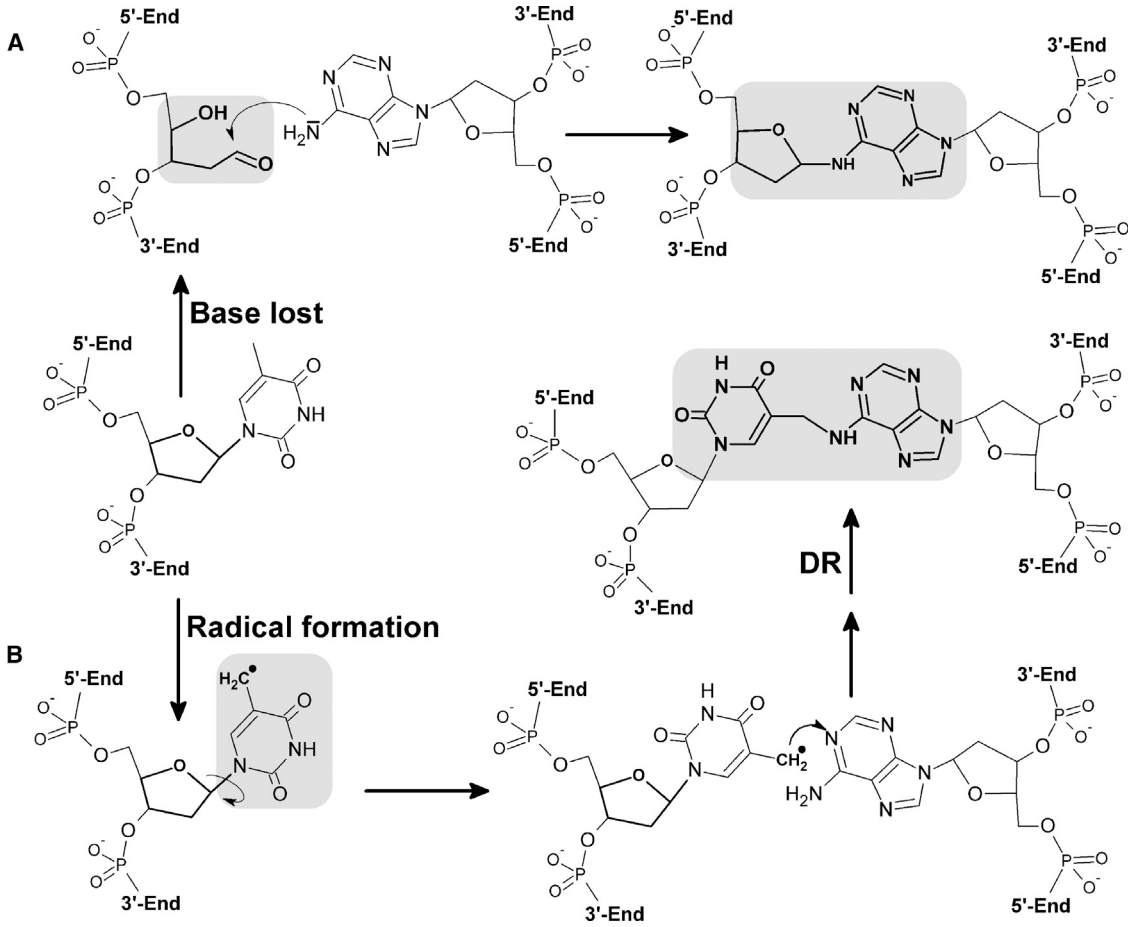


**Figure 2. DNA Interstrand Cross-Link Formation**

(A and B) DNA interstrand cross-link formation via (A) aldehyde for of apurinc/apyrimidinic site and (B) radical mechanism with Dimroth rearmament (DR).[23]

of view, the methylene bridge between thymine and adenine makes the system less energetically favorable by 165.31 kcal•mol$^{-1}$ and more rigid than the native AT base pair in the context of the double helix. These significant energetic differences derived from the nature of the AT cross-link under discussion. The isolated AT-ICL was 136.46 kcal•mol$^{-1}$ higher than the native AT nucleoside pair energies. For the discussed optimized structures, no imaginary frequencies were found, which is clear evidence that both the discussed molecules are at an energetic minimum. Additionally, as shown below, the energetic differences between dsDNA and ICL-DNA were increased by the interaction between the ICL moiety and the adjacent 3′ end and 5′ end base pairs. This interaction leads to a flattening of the AT-ICL structure.

The preliminary theoretical study showed that the AT-ICL is not a linear molecule but adopts a bent geometry (Figure 3). The rotation of the thymidine moiety around the new C5-N6 thymine-adenine bond results in two stable conformers, in which the pyrimidine ring adopts a spatial position on the site of 5′O or 3′O of the adenosine subunit, denoted as AT-ICL$^{-}$ and AT-ICL$^{+}$. The results of DFT calculation, in terms of energy, revealed that these two forms of isolated ICL are almost equal, i.e., $\Delta E$ = 0.31 kcal•mol$^{-1}$, with an indication on AT-ICL$^{+}$. Moreover, an analysis of internal structural parameters, presented in Table 1, did not show notable differences, apart from a dihedral angle determined by $C6^{Ade}$-$N6^{Ade}$-$C5^{MThy}$-$C5^{Thy}$, which adopted the same value of 78° with opposite signs. Moreover, the discussed mutual spatial orientation adenine versus thymine, within AT-ICLs, caused a difference in dipole moment (DM) value of 2.5 [D].

It is important to mention here that the 2′-deoxyribose ring, derived from the adenosine part of the AT base pair and both forms of AT-ICL$^{-/+}$, adopted close values of phase and amplitude, i.e., ∼178° and ∼34°, respectively. The same parameters calculated for the thymidine sugar ring adopted a higher value for the native nucleoside pairs than for the corresponding AT-ICLs. The results are given in Table 1. As shown in Figure S1 , the three-dimensional geometries of AT-ICL are significantly different from the canonical AT base pair. The structure varieties were well reflected by DM values, which implies the changes in the electronic parameters of the discussed systems (Figure S2).[32] A careful analysis of the adiabatic and vertical

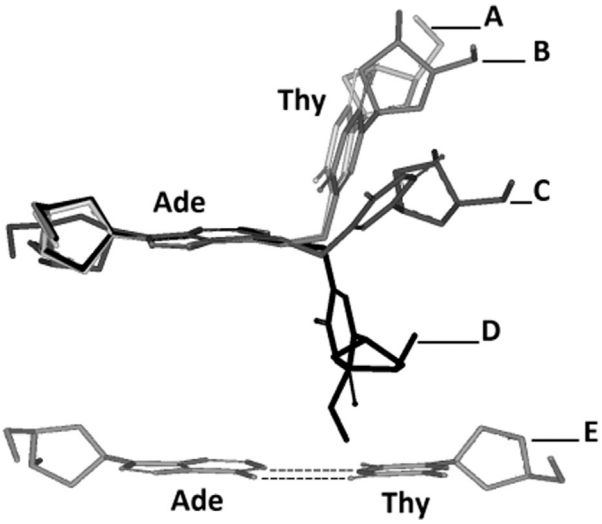


**Figure 3. Comparison of Obtained AT Interstrand Cross-Link**

(A–E) Comparison of obtained AT interstrand cross-link 3D structures after geometry optimization on M062x/6-31+G** level of theory in aqueous phase as follows: (A) AT-ICL$^{-}$ as isolated molecule, (B) AT-ICL$^{R}$ extracted from dsDNA, (C) AT-ICL extracted from double-helix structure without further optimization, (D) AT-ICL$^{+}$ as isolated molecule, and (E) canonical d[A]*d[T] pair.

ionization potentials (AIP and VIP), surprisingly, did not indicate any influence of methylene bridge on the aforementioned parameters. The situation was the reverse in the case of the adiabatic and vertical electron affinities (AEA and VEA). These values were found to be higher for AT-ICL$^{-/+}$ than for those of the native AT base pair. The values of discussed electronic parameters are presented in Table 2.

Based on the obtained results, as well as on calculated vertical electron attachment and detachment energy, it can be concluded that the appearance of AT-ICL in the genome structure can play a significant role on electron transfer through dsDNA. Contrary to that, the hole (radical cation) migration within the double helix should be unaffected by the presence of ICL moieties.

### The Influence of the Stacking Interaction on AT-ICL Structure

To elucidate the above hypothesis, the AT-ICL was localized in the central part of short double-stranded oligonucleotide, i.e., d[AGA$^{ICL}$G]*d[CT$^{ICL}$CT]. Due to the high complexity of the system, a QM/MM strategy was used for geometry optimization.[33] The internal part of the double helix was described by DFT, while the sugar phosphate backbone by universal force field (UFF) for the theoretical investigation. This approach makes the calculation in the condensed (aqueous) phase less time consuming (and less expensive), with reasonably accurate maintenance of the obtained results. It is important to mention that, for the DFT part, all the geometry optimizations were performed at this M062X/6-31+G* level of theory.[34] Developed by the Truhlar functional, this, as has been shown previously, is dedicated to noncovalent interaction energies, such as stacking, HBs, etc.[35] Moreover, thanks to the above, the energy, charge, and spin distribution, in addition to the DM of complete investigated systems, were obtained at the same DFT level of theory (M062/6-31+G*).

As shown in Figure 3 and described in Table 1, the structure of the AT ICL was significantly different from the native adenosine thymidine base pair. As expected, these observations were embodied in a DM value in Debyes as follows: 2.92, 5.11, and 7.60 of neutral AT, AT-ICL$^{-}$, and AT-ICL$^{+}$, respectively. It was assumed that the lower DM value provides a higher geometrical fluctuation of molecules and vice versa.[36] Moreover, the above data suggest a different character of excess electron attachment to a neutral system and of a subsequent anion, i.e., covalent or dipole bond.[37–39] Hence, the DM can be a valuable parameter for the description of changes in the geometry of dsDNA during the charge migration.

In 1953, Watson and Crick[40] published the results of their work on the dsDNA structure. Since that time, the spatial geometry of double helix has been well described by standard reference frame parameters as well as internal factors, such as stacking interaction and HB energies between complementary and adjacent nucleobases.[41] It is important to mention here that the 3D structures of ideal models of AT and GC pairs are different from those obtained from suitable base pairs extracted from dsDNA.[42,43] These observations suggest that even small changes in the nucleoside moieties can lead to a noticeable fluctuation in the dsDNA structure, which can be partially compensated by the sugar phosphate backbone's flexibility. Therefore, based on the above data, the appearance of the ICL in the ds-oligonucleotide should influence the double-helix geometry parameters.

As presented on Figure 3, both structures of the free ICL AT-ICL$^{-/+}$ show spatial differences to those obtained for the native AT base pair. Therefore, a significant influence on dsDNA's three-dimensional structure can be expected. Surprisingly, the results of geometry optimization of d[AGA$^{ICL}$G]d[CT$^{ICL}$CT ds-oligonucleotide, using QM/MM strategy in the aqueous phase, did not elucidate a significant fluctuation compared to the native one, i.e., d[AGAG]d[CTCT]. Moreover, a comparison of the structure of the extracted adenine-thymine ICL from the investigated dsDNA with the structure of optimized AT-ICL$^{+/-}$ gave a different view. This observation indicated that the stacking interaction between AT-ICL and neighboring base pairs forces the flattening of the cross-link structure, as shown in Figure 3.

As can be expected, the secondary AT-ICL (derived from dsDNA) geometry optimization led to its structure relaxation, denoted as AT-ICL$^{R}$. The difference in energy between the final (relaxed) and initial (stretched) forms was −41.8 kcal•mol$^{-1}$. The release of AT-ICL from the pressure of adjacent base pairs led to structure bending similar to that of AT-ICL$^{+}$ (Figure 3; Table 1). The diagnostic dihedral angle N1$^{Ade}$-C6$^{Ade}$-C5$^{MThy}$-C5$^{Thy}$ adopts the following values: −74.7°, −75°, 62.7°, 36.1°, and −0.7° for AT-ICL$^{+}$, AT-ICL$^{-}$, AT-ICL$^{R}$, AT-ICL, and AT, respectively. However, although all the base pair parameter values between AT-ICL$^{+/-}$ and AT-ICL$^{R}$ were largely

**Table 1. Structural Parameters of Single Base Pair, after Geometry Optimization on the m062x/6-31+G* Level of Theory in Aqueous Phase**

| Parameter | dA::dT | AT-ICL$^{-}$ | AT-ICL$^{+}$ | AT-ICL$^{R}$ |
|---|---|---|---|---|
| L (Å) | 9.89 | 6.93 | 6.93 | 7.09 |
| D1 (Å) | 8.94 | 7.51 | 7.60 | 7.91 |
| D2 (Å) | 10.69 | 9.23 | 9.27 | 9.71 |
| λ(I) (°) | 53.65 | 46.21 | 44.64 | 43.82 |
| λ(II) (°) | 52.53 | 60.86 | 63.40 | 58.92 |
| λ(III) (°) | −5.77 | −24.36 | 19.44 | −22.90 |
| HB-1 (Å) | 2.96 | 3.15 | 3.15 | 3.21 |
| HB-2 (Å) | 2.90 | 5.19 | 5.15 | 5.48 |
| G(Pu)/G(Py) (Å) | 1.45/1.46 | 1.45/1.46 | 1.45/1.46 | 1.46/1.47 |
| P(Pu)/P(Py) (°) | 177.84/ 169.76 | 177.58/ 146.51 | 178.29/ 135.50 | 175.88/ 51.46 |
| A(Pu)/A(Py) (°) | 33.93/ 35.22 | 34.20/ 41.31 | 34.00/ 42.56 | 31.17/ 36.31 |
| $N1^{Ade}$-$C6^{Ade}$-$C5^{MThy}$-$C5^{Thy}$ (°) | −0.7 | 75 | −74.7 | 62.7 |

Pu, purines; Py, pirymidines; G, glyosidic bond; P, sugar ring puckering; A, sugar ring amplitude; L, $C8^{(Pu)}$-$C6^{(Py)}$; D1, $N9^{(Pu)}$-$N1^{(Py)}$; D2, $C1'^{(Pu)}$-$C1'^{(Py)}$; λ(I), $N9^{(Pu)}$-$C1'^{(Pu)}$-$C1'^{(Py)}$; λ(II), $N1^{(Pu)}$-$C1'^{(Py)}$-$C1'^{(Pu)}$; λ (III), $N9^{(Pu)}$-$C1'^{(Pu)}$-$C1'^{(Py)}$-$N1^{(Py)}$.

comparable, the sugar puckering of the thymidine moiety of AT-ICL and AT-ICL$^{R}$ was different from the others and adopted a $_4T^3$ conformation instead of $_1T^2$. Additionally, these differences were not observed for the complementary purine part of the duplex. The base pair parameters are presented in Table 1. The anomalous geometry of the AT ICL versus the native AT base pairs should lead to differences in electronic properties, i.e., AIP, VIP, VEA, and AEA. Moreover, the attachment of an excess electron or electron loss should be noticeable in the DM changes.

### Electronic Property Comparison

The obtained results presented in Table 2 show comparable adiabatic and VIP values between the reference AT base pair and the three forms of AT-ICL. For the above parameters, the higher difference was found to be 0.05 eV. The situation was opposite in the case of adiabatic and vertical electron affinity (VEA) descriptors; the discussed cross-links adopted a higher value than that of the the native AT base pair in a perceptible range of about 0.1 eV (Table 2). Therefore, it can be expected that the AT-ICL will form a more stable anion with a longer lifetime than a native AT pair.

Using the same level of theory, the ionization potential of dG:::dC (5.79 eV) was found to have the lowest value, which is in accordance with common knowledge.[44] As mentioned above, the changes of DM were significantly denoted in the case of the electron attachment process; its increases for AT-ICLs in comparison to AT by 4.49[D] (AEA) and 7.03 D (VEA) were observed. The adoption, by all the discussed ICL molecules, of high DM values above 10 [D] suggests the formed anion was of a dipole bond character rather than a covalent one.

### Influence of the AT-ICL on dsDNA Electronic Properties and the Charge Transfer Process

The DNA double helix from its nature can be perceived as nanowire.[45] It is well known that a cation radical migrates through ds-oligonucleotide at a distance of up to 200 Å by a hopping mechanism or over a few base pairs by a tunneling effect.[46] The latter is derived from the de Broglie wave nature of electrons.[47] In both the above cases, the mutual base pair position as well as their individual electronic properties are crucial for the charge transfer process. As a result, the DNA lesion appearing in the double helix possesses the probability potential to upset the electron or hole migration through double-stranded nucleic acids. For example, Schuster and colleagues[48] have shown that the presence of 8-oxo-dG, the lowest ionization potential value, in the double helix constituted the place of radical cation stabilization, i.e., the stopping point for further charge migration. Therefore, DNA damage can influence the charge migration by its electronic properties, such as ionization potential and electron affinity, without significant changes to the base pair stacking interaction. On the other hand, the lesion-like inter-intrastrand cross-link or 5′,8-cyclo-2′-deoxypurines upset the internal or global helix geometry parameters, which are forced by the presence of an additional covalent bond.[27,49] In the latter case, the structural factor can be more important than the electronic factor for the charge migration through dsDNA due to, for example, increases in the distances between the stacked base pairs (containing lesions), which can be propagated over several neighboring nucleotide units.[50]

### Double-Helix Geometry Changes during the Charge Transfer

According to the Standard Reference Frame for the Description of Nucleic Acid Base-pair Geometry, the structure of the double helix can be described by six local base-pair steps (shift, slide, rise, tilt, roll, and twist) and six local base-pair parameters (shear, stretch, stagger, buckle, propeller, and opening).[41] Table S1 presents the adequate values calculated for dsDNA with and without the ICL. The graphical representation of the AT-ICL's influence on the double helix is shown in Figure S3 as the differences of parameter values between native and lesioned DNA. The comparative conformational analyses show that the interstrand covalent (C5-N6) linkage of complementary adenine thymine base pairs force noticeable changes, mainly in the place of the cross-link formation (i.e., $A_2T_2$) in the case of neutral molecules. Moreover, the propagation of the AT-ICL disruption effect was noticeable in the 3′ end direction of the purine strand, while the part of the double-stranded DNA on the 5′ end remained less affected. The above trends in parameter changes were also noted for the discussed oligonucleotide after a suitable anion or cation formation. These observations were evident after comparison changes in both the local base-pair step and local base-pair parameters obtained for the native and cross-linked double helix after electron attachment or electron loss (Figure S4; Tables S1 and S2).

Based on these observations, it can be concluded that dsDNA structural distortion forced by an additional electron or electron deficit are mostly at the same level for unaffected and cross-linked dsDNA, except for the twist, tilt, and buckle parameters. The electron appearing in the system

**Table 2. Electronic Properties of Single Nucleosides Pairs**

| | Single Nucleoside Pair | | | |
|---|---|---|---|---|
| | dA::dT | AT-ICL$^{-}$ | AT-ICL$^{+}$ | AT-ICL$^{R}$ |
| DM$^{Neutral}$ | 2.92 | 5.11 | 7.60 | 6.19 |
| VEAE | 5.96 | 5.94 | 5.96 | 5.95 |
| DM$^{VEAE}$ | 4.47 | 2.67 | 5.91 | 5.03 |
| VEDE | −2.45 | −2.63 | −2.64 | −2.63 |
| DM$^{VEDE}$ | 4.53 | 3.93 | 5.97 | 4.11 |
| VIP | 6.58 | 6.50 | 6.50 | 6.51 |
| DM$^{VIP}$ | 11.63 | 10.17 | 11.89 | 14.32 |
| AIP | 6.28 | 6.22 | 6.22 | 6.23 |
| DM$^{AIP}$ | 11.90 | 10.98 | 12.15 | 15.31 |
| VEA | 1.43 | 1.53 | 1.55 | 1.52 |
| DM$^{VEA}$ | 16.09 | 19.22 | 23.12 | 20.27 |
| AEA | 1.88 | 2.02 | 2.02 | 2.00 |
| DM$^{AEA}$ | 14.58 | 16.27 | 19.07 | 17.09 |
| NER1 | 0.29 | 0.28 | 0.28 | 0.29 |
| NER2 | 0.32 | 0.27 | 0.27 | 0.27 |
| NER3 | 0.45 | 0.49 | 0.46 | 0.48 |
| NER4 | 0.57 | 0.62 | 0.63 | 0.63 |

triggers higher changes in these descriptors than after radical cation formation. The difference in twist, tilt, and buckle derived from native and ICL ds-oligonucleotides adopted values in the range as follows: tilt, 9.28/−5.32 and 2.17/−1.88; twist, 1.33/−6.97 and 1.62/−3.43; and buckle, 25.97/−10.8 and 13.89/−2.50 for the anionic and cationic forms, respectively (Table S2; Figure S4).

As discussed below, the above notifications are related to the radical distribution. The position of the mutual nucleic bases in the complementary nucleoside pair can be described by several structural factors, namely, HB length; energy ($E_{HB}$); distances L, D1, and D2; and angles λ(I) and λ(II).[28,41] Additionally, the sugar moieties of the discussed system can be characterized by the puckering and amplitude parameters.[30] Furthermore, the length of the glyosidic bond can be used as a valuable criterion of the nucleoside geometry fluctuation and nucleoside stability under charge migration. As presented in Table S1, significant differences in HB length between native dsDNA and dsDNA containing the AT-ICL were noted for the position of the base pair and corresponded to the AT-ICL for the cation, neutral, and anion forms of the discussed ds-oligonucleotides. These differences are derived from the fact that the AT-ICL thymine ring was rotated by 180° around the glycosidic (a *syn* conformation) bond compared to the native one (an *anti* conformation). The same was observed for the other parameters: the appearance of the AT-ICL led to a shortening of L, D1, and D2; decreases in the λ(I) angle; and increases in the λ(II) angle (Table S1).

Surprisingly, the comparison of the above parameters obtained for the remaining base pairs, i.e., $A_4T_4$, $G_3C_3$, and $G_1C_1$ in native and lesioned dsDNA, did not demonstrate significant differences. A comparative analysis of native dsDNA with cross-linked dsDNA showed in all the discussed nucleoside pairs that differences in glycosidic bond lengths are almost unaffected by the presence of the AT-ICL or by electron attachment to or detachment from ds-oligonucleotides. For nucleosides derived from both strands, the differences were found at the level of 0.01 Å. Only in the anionic form of the $G_1C_1$ system was a greater shortening by 0.016 Å of glycosidic bond in the cytidine moiety noted. The above observations are in good agreement with differences in HB energy (Table S1).

For the oligonucleotides in the neutral and cationic states, the HB weaknesses were observed for G:::C pairs with subsequent A::Ts unaffected. Interestingly, compared to the neutral form, this difference was more visible for the $G_3C_3$ after cation formation by dsDNA, with increases of 0.11 kcal•mol$^{-1}$. Surprisingly, in the same case, the $\Delta E_{HB}$ for the $G_1C_1$ system decreased by 0.2 kcal•mol$^{-1}$. The electron attachment by the double helix (anionic form) led to the difference in HB energy of the base pairs ($G_3C_3$ and $A_2T_2$) in the central part of compared ds-oligonucleotides (Table S1). The decreases of $\Delta E_{HB}$ for the $A_4T_4$ pair up to −0.54 kcal•mol$^{-1}$ and increases for $G_1C_1$ to 0.47 kcal•mol$^{-1}$ are derived from the spin and charge distribution in the anionic form of native and lesioned dsDNA.

As presented above, the appearance of an additional covalent bond in the discussed AT ICL forces some structural changes in the double helix. These changes concern mainly the difference between the AT-ICL and corresponding $A_2T_2$ base pair in unaffected dsDNA. The smaller-than-can-be-expected structural influence of the discussed AT-ICL on the spatial ds-oligonucleotide geometry revealed the crucial role of sugar phosphate backbone flexibility on change compensations. A comparison of the two sugar moiety parameters puckering and amplitude confirms the above postulate. As shown in Table S1, the significant differences in values of these descriptors were observed for all the furanose rings in both DNA strands in the cation, neutral, and anion dsDNA forms. It is important to mention here that the sugar moiety of adenosine and thymidine in the AT-ICL adopted 98.2/49.2, 110.1/52.4, and 106.8/64.6 phases instead of 154.5/122.8, 153.8/137, and 151.3/110.8 (all values in degrees) for native AT pair in neutral, cation, and anion dsDNA forms, respectively). Subsequently, in all cases (for each nucleoside in the discussed systems), the amplitude fluctuated at the range of 27.7°–36.4°, giving a difference between undamaged and damaged dsDNA up to ±5°. The above results are presented in Table S1.

Due to the fact that sugar phosphate can be noticed as the DNA spine, its changes in one place can induce and propagate fluctuation in a further part of ds-oligonucleotide in both the 5′ and 3′ end directions. The backbone of the double helix is described by six dihedral angles, as depicted on the graph in Table S3. A comparative analysis of native dsDNA and dsDNA containing AT-ICL in their neutral, cation, and anion forms has shown that, for both pyrimidinic and purinic strands, δ and ζ angles are the most sensitive to the AT-ICL presence (Figure S1). For the four remaining dihedral angles, the higher fluctuation

was observed in the pyrimidine strand. Moreover, the chances of mutual orientation between the furan ring and adequate nucleic base was well visible only for the thymidine moiety of the discussed AT cross-link ($\Delta\chi$ ~200°). Based on these observations, it can be concluded that adaptability of the double-helix sugar phosphate backbone served as a shock absorber for the changes triggered by DNA damage.

### Stacking Interaction

The DNA lesions, which are characterized by significantly higher distortions, can lead to a greater local duplex destabilization and influence base-base stacking interactions. From a biological point of view, it should be pointed out that, the greater the stacking impairment force, the greater the relative NER efficiency.[51] The three-dimensional structure of ds-oligonucleotides is maintained by two types of interhelix interactions: HBs between complementary bases and a less obvious stacking interaction.[52] The latter plays a crucial role in charge transfer, due to the fact that it can be perceived as a spatial pronunciation effect of orbital, charge, and spin localization.[53] It should be pointed out that not only is the structure of dsDNA subjected to continuous dynamic fluctuation but also the above-mentioned elements. Due to their different pattern within double-stranded oligonucleotides, the stacking interactions in anionic and cationic shapes force their analyzed and discussed-as-suitable vertical neutral forms. These approaches leave the adiabatic cation or anion spatial molecule geometry with subsequent charge neutralization. Moreover, the proposed idea appositely supplements and describes the electron or hole migration process over the double helix.

The stacking interaction can be discussed as a sum of the interstrand (IN) or intrastrand (IT) relationship between nucleic bases depicted in the scheme in Table S4. A comparative analysis showed that the appearance of the AT-ICL in the genome visibly disturbs the interaction in the place of its formation and transferred to the 5′ end direction of adenosine in neutral ds-oligonucleotide forms (Figure S5B; Table S4). The highest differences were noted for IN-3 and IN-4, i.e., 1.3 and 2.88 kcal•mol$^{-1}$, respectively. It is important to mention here that stacking interactions are weak interactions, with a total energy of around several kcal•mol$^{-1}$.[52] On the other hand, the calculation accuracy of Minnesota Density Functional DFT (M06-2X) for the non-covalent interaction was found to be at the level of 0.43 kcal•mol$^{-1}$.[54] These two limitations make the analysis very difficult. Fortunately, as shown below, the reasonable differences in interastrand stacking interactions between native and cross-linked dsDNA equal around 1–2 kcal•mol$^{-1}$, which corresponds to 25%–40% of its energy changes. Such a high fluctuation, in percentage, of base-pair stacking indicates its susceptibility to the presence of ICL in the structure of the double helix. Additionally, these observations are in good agreement with the roll and twist parameters calculated for suitable base pairs (Table S2), which denoted the overlap of purine and pyrimidine rings. The loss of an electron by the system leads to a cation radical formation. Similar to previously, the destabilization effect of the AT cross-link was observed for its interaction with the $G_3C_3$ base pair (IN-3 and IN-4) and IN-5 between $A_2$ and $G_1$, leaving the rest of ds-oligonucleotide almost unchanged (Table S4) for the suitable pseudo-cations. It is important to mention here that the shapes of curves, which represent the intrastrand stacking interaction in the native dsDNA and ICL-DNA, are similar (Figure S5C).

It is indicated that the radical cation should be located at the same place of the double helix. The additional electron appearing in the system leads to different consequences (Figure S5A). In the case of undamaged dsDNA, decreases of 1.45 kcal•mol$^{-1}$ in IN-2 stacking energy were observed between the pyrimidines T4/C3 and 1.38 kcal•mol$^{-1}$ (IN-5) for purines A2/G1 of ICL-DNA, with subsequent energy increases between T2/C1 (IN-6). Therefore, the changes of base spatial interactions between the neutral and pseudo-anion forms suggest a differentiation in negative charge localization. The compression of the interstrand interaction between native and cross-linked DNA in their neutral, pseudo-anion, and pseudo-cation revealed differences between them (Table S4). In the neutral form, AT-ICL impaired the interstrand interactions IT-1, IT-4, and IT-5 and reinforced IT-2 and IT-3, with subsequent IT-6 leaving at the same level in comparison to native ds-oligonucleotide. The analysis of the mentioned dsDNAs in pseudo-anion form showed the different effects of an additional electron appearing in the double helix. For the undamaged dsDNA, increases of the IT-5 interaction of 0.28 kcal•mol$^{-1}$ with subsequent IT-4 decreases of 3.53 kcal•mol$^{-1}$ were observed, while in the cross-linked case, a stabilization effect of 1.32 kcal•mol$^{-1}$ was noted for IT-3 (Table S4). The rest of the ITs were found to be almost at the same level. The loss of electron by the double helix in both cases of oligonucleotides led to decreases in interstrand interaction in the same region of the system (from IT-1 to IT-4). Therefore, as previously, it can be concluded that the radical cation should be located in the same place of dsDNAs contrary to that radical anion should be located in a different area of native and lesioned ds-oligonucleotides. Finally, it was found, that far spatial inter- or intrastrand interactions IT-7–IT-10 and IN-7–IN-10 were resistant (not sensitive) to adenine thymine, the interstrand cross-link presence in the system, which is focused on in Table S4.

### Charge and Spin Distribution

The influence of DNA damage on the charge layout has mainly been discussed at the level of isolated base pairs or nucleoside pairs. Based on data, it can be concluded that purines mainly adopt a positive charge while pyrimidines adopt a negative one.[55,56] These valuable studies are helpful for the discussion on proton-charge transfer process within a simple canonical model. The system extension from the base and nucleoside pairs to short double-stranded oligonucleotide adds a parameter, namely, stacking (the through-space aromatic ring interaction). Therefore, dsDNA losing or accepting an electron leads to a suitable anion or cation formation within the system. Depending on the three-dimensional geometry of the double helix, the hole or negative charge can migrate along the strands, in both directions, exploiting the nature of stacked bases.[46,57] A charge distribution analysis of the [AGAG]*[CTCT] neutral form revealed that, in canonical double-stranded DNA, almost equally, vestigial negative charges are located on AT pairs, with positive ones on GCs.

The situation is different in the case of cross-linked DNA, though. The additional covalent linkage between adenine and thymine leads to partial negative charge accumulation on the AT-ICL, with subsequent positive charge delocalization on the $G_1C_1$ pair. The remaining $G_3C_3$ base pair on the 5′ end direction, in regard to $A_2$ moiety, was noted as roughly neutral. Moreover, decreases in the negative charge on $A_4T_4$ versus uncross-linked DNA were observed. It is important to mention here that, on the 3′ end direction, determined by the adenine of the AT-ICL, purines showed a higher sensitivity to the AT-ICL appearing in the structure than on the 5′ end pyrimidines (Table S5A). The initial electron loss (vertical radical cation state) led to a positive charge dispersion over the $G_3C_3$ neighborhood, as shown in Table S5A and Figure S6B. In the case of the AT-ICL, the hole in the vertical state was mainly located on the $G_3G_3$ base pair. A more detailed analysis showed that all bases apart from thymines in native dsDNA adopted a positive charge, forming the tract for hole migration on the dsDNA highway, while the AT cross-link formation in the ds-oligonucleotide forced a positive charge accumulation over all the bases on the 5′ end part of dsDNA above the AT-ICL (Table S5A). Therefore, in this situation, it can be concluded that an AT-ICL can disturb the positive charge transfer along the double helix in the adenine ($A_2$) 3′ end direction. Surprisingly, after electron rearrangement and adiabatic cation state achievement by systems in both cases, the positive charge was localized in the $G_3C_3$ base pairs. Moreover, a comparison of charge distribution within native and lesioned dsDNA revealed almost the same profile as depicted in Figure S6C.

These observations suggest that, even though the mechanism of hole transfer is different for the native and cross-linked DNA, the final place where the radical cation settles will be the same. The dissimilarity of the discussed process was supported by the charge distribution after charge neutralization by electron attachment to the double helix (neutral vertical state) Figure S6D. An analysis of the charge distribution within native dsDNA indicated the reconstitution of its localization as in an adiabatic neutral form. Surprisingly, the presence of the AT-ICL in the double helix caused the charge distribution as found in the vertical cation state, except guanine of $G_3C_3$, which changed the charge from +0.697 to −0.247 (Table S5A). These results indicate that, during the hole transfer process, in the presence of the AT-ICL, $G_3$ plays crucial roles: from one site guanine can adopt the role of electron donator, from the other electron acceptor.

The additional electron attachment to the system leads to its vertical anion formation. The data presented in Table S5B and Figures S7A–S7D show the differences in negative charge distribution within native and cross-linked dsDNA. In the vertical anion form, the captured electron was dispersed over all the nucleobases of the native system apart from adenines $A_4$ and $A_2$, which adopted a slightly positive (close to zero) charge of +0.009 and +0.023, respectively. The appearance of the additional covalent bond (AT-ICL) in the double helix leads to different vertical anion locations (Figure S7B). In the cross-linked dsDNA, the negative charge was found mainly on the thymidine moiety (−0.632) belonging to the AT-ICL. Moreover, the spatial position of the cross-link divided the ds-oligonucleotide into two parts: positively charged on the 5′ end site of $dA_2$ and negatively on the $dA_2$ 3′ end direction, as shown in Table S5B. This dissimilarity between the vertical anion of the native and lesioned double helix leads to different natures of the subsequent adiabatic anions (Figure S7C). The negative charge in dsDNA is mainly located on the thymine $T_4$ (−0.895) of $A_4T_4$, while within ICL-DNA it is on $C_1$ (−0.637) of $G_1C_1$. This observation suggests the different direction of negative charge migration between undamaged and lesioned ds-oligonucleotide, i.e., in native dsDNA the anion migrates to the 5′ end site, while the AT-ICL forces the anion migration to oligos' 3′ end, determined by $dA_2$. The negative charge (excess electron) disappearing from the part of the discussed systems leads to the formation of their suitable neutral vertical forms. Surprisingly, in both the discussed cases, the charge distribution showed a shape resembling each other (Figure S7D). A high difference was found for thymine's $T_4$, which adopts the following values: +0.318 and +0.016 for ICL-DNA and dsDNA, respectively.

### Molecular Orbital and Spin Distribution

The loss of a valence electron and cation radical formation force changes in the low-unoccupied (LUMO) and high-occupied molecular orbital (HOMO) localization.[23,58] As mentioned above, this process passes through a vertical state, the view of related LUMO indicated its *in situ* place of formation. The subsequent nuclear reorganization leads to an adiabatic anion with adequate HOMO reorganization. The difference between the vertical and adiabatic LUMO localization can indicate the path of hole transfer within the system. As shown in Figure 4, the presence of the AT cross-link within the dsDNA dramatically changes the migration process. In the case of ICL-DNA, the vertical radical cation was formed at a strictly defined place on the $G_3$ of the $G_3C_3$ base pair, which is the destination point of the adiabatic cation's location. The situation is the reverse for native dsDNA: the cation radical migrated from the dispersed vertical state over $G_1C_1$, $A_2$, and $C_3$ to its final adiabatic location on $G_3C_3$. It is important to mention here that the HOMOs were settled on the opposite sides of native and cross-linked dsDNA, i.e., on $G_4$ and $G_1$ nucleobases in their vertical state. Following the nuclear rearrangement process, HOMO was found at the same place of both the discussed molecules, i.e., on $G_1C_1$. Therefore, from the above results it can be concluded that the AT-ICL, despite the lack of LUMO dispersion, is not a point resistant to the hole migration process through double helix.

On the other hand, the electron attachment to the neutral system of native dsDNA was initially located on LUMO, which in the vertical anion state transformed into HOMO. As shown in Figure 4, the HOMO of the anion in its nascent state was dispersed over all the pyrimidines, except for $T_4$. Such an electron blur suggests that the initial negative charge can migrate almost unperturbed through the double-helix pyrimidine track. This postulate can be supported exclusively by the HOMO localization on $T_4$ belonging to the $A_4T_4$ base pair in the adiabatic anion. The presence of the AT-ICL in the dsDNA structure caused an additional electron location in the more restricted area. The HOMO of the vertical anion settled only on $T_2$ of the AT-ICL and on

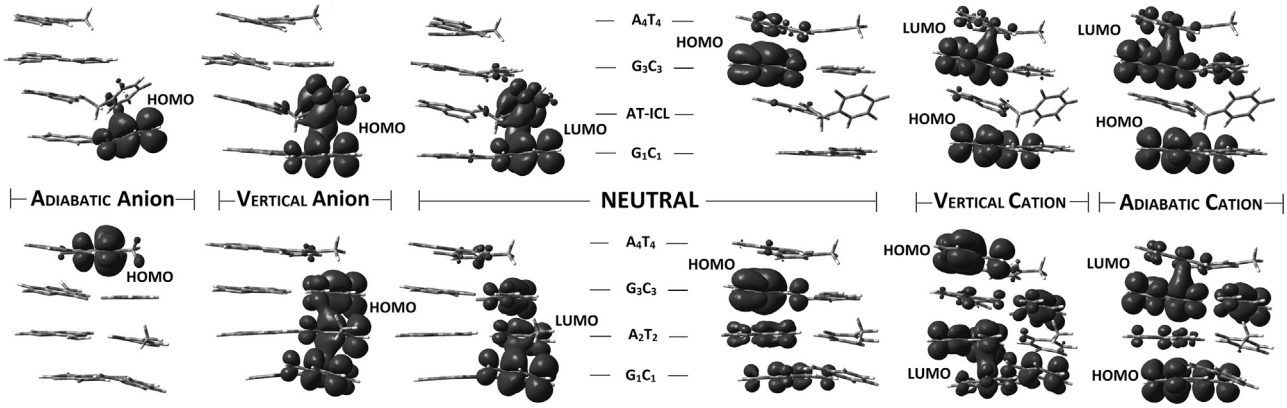


**Figure 4. HOMO and LUMO of Neutral, Cationic, and Anionic Forms of [AGAG]*[CTCT] and Cross-Linked [AGA$^{ICL}$G]*[CT$^{ICL}$CT], Calculated on the M062x/6-31+G* Level of Theory in Aqueous Phase**

$C_1$ of the $G_1C_1$ pair. After nuclear rearrangement, the HOMO of the adiabatic anion was found on the $G_1C_1$ base pair instead of $A_4T_4$ of native dsDNA. These differences indicated that the discussed ICL effectively stopped the negative charge migration in the 5′ end direction defined by adenine ($A_2$).

The charge dispersion discussed above is inextricably linked to spin distribution (Figures 5A–5C; Table S5A and S5B). In the case of the vertical cation dsDNA, the spin distribution revealed that a loss of electron occurs at the $G_1$ (0.394), $A_2$ (0.213), and $G_3$ (0.386) moieties. The subsequent nuclear rearrangement led to it settling at $G_3$. In the case of cross-linked dsDNA, the electron ejection occurs solely from the terminal radical location $G_3$. On the other hand, the unpaired electron (spin) in vertical anion radical is distributed over the $C_1$(0.29), $T_2$(0.82), $C_3$(0.41), $T_2$(0.56), and $C_1$(0.18) nucleobases of native dsDNA and ICL-DNA, respectively. The system relaxation after the appearance of an additional electron forces the radical migration to the final appropriate destinations $T_4$, $C_1$, and $T_2$ of native and cross-linked dsDNA. The graphical representation of the spin distribution comparative analysis dsDNA versus ICL-DNA is presented in Figure 5B.

### Electronic Properties of Native and Cross-Linked dsDNA

As shown above, the radical cation is mainly formed in both the discussed native and cross-linked dsDNAs on purine moieties, while the radical anion forms on pyrimidines. These results are in good agreement with Sevilla's previous studies, which showed that, during oligonucleotide γ-radiation, the following amounts of suitable radicals are formed: 35% $G^{\bullet+}$, 5% $A^{\bullet+}$, and about 45% of $T^{\bullet-}$ and $C^{\bullet-}$.[59] The electronic properties of nucleic bases, nucleosides, and base and nucleoside pairs have been intensively studied during the last decades using theoretical and experimental methods.[60,61] However, there are no data concerning the AT-ICL under discussion in this paper and hardly any about other DNA lesions, mainly 8-oxoG.[62,63] The comparison of theoretically estimated VIP or AIP and electron affinity of isolated nucleoside pairs (dG:::dC and dA::dT) with those obtained for the three different forms of AT-ICL elucidates the influence of the additional covalent junction on electronic properties (Table 2).

The presence of the AT-ICL in the short dsDNA under investigation did not lead to changes in its resultant globalAIP, and there was scant evidence of changes in the VIP calculated at the same level of theory (Table 3).

For native and cross-linked dsDNA, the following values (in eV) were found (VIP/AIP): 6.32/5.67 and 6.15/5.71. These results suggest that the cation radical formation process is slightly privileged in the case of the discussed ICL-DNA, which was confirmed by spin and HOMO/LUMO distribution analysis. From the other point, the VEA adopts almost the same value for both ds-oligonucleotides; the difference was found to be 0.06 eV. However, a comparison of AEAs showed some difference as it turned out that the ICL-DNA adopts higher values by 0.27 eV than unmodified dsDNA. As shown above, the AT-ICL can form a more stable anion with a longer lifetime than the native adenine thymine pair. Therefore, it can be postulated that some part of ds-oligonucleotide containing the investigated type of cross-link is able to stop or slow down electron transfer. The electronic parameters of the double helix are presented in Table 3. The share of sugar phosphate backbone in electronic properties was estimated as follows (in eV): (1) ionization potentials decrease, VIP by 0.25/0.35 and AIP by 0.34/0.35; and (2) electron affinity decreases, VEA by 0.79/0.52 and AEA 0.62/0.51 of native/cross-linked dsDNA, respectively. The data presented above would indicate some influence of the double-helix spine on the charge migration process, which is in agreement with previous studies.[64]

The base pairs interact not only between each other (HBs) in the double helix but also with neighboring pairs by stacking interaction, which influences changes in both its spatial geometry and electronic properties. As a result, the assignment of VIP or AIP and electronic affinity of isolated base pairs from native and cross-linked dsDNA is vital for understanding the charge transfer through the double helix. To assign the influence of sugar moiety on suitable parameters, calculations were performed for base and nucleoside pairs. (As shown in Table 3, no significant differences were found, thus the base pair systems were taken for further consideration.) Among all the

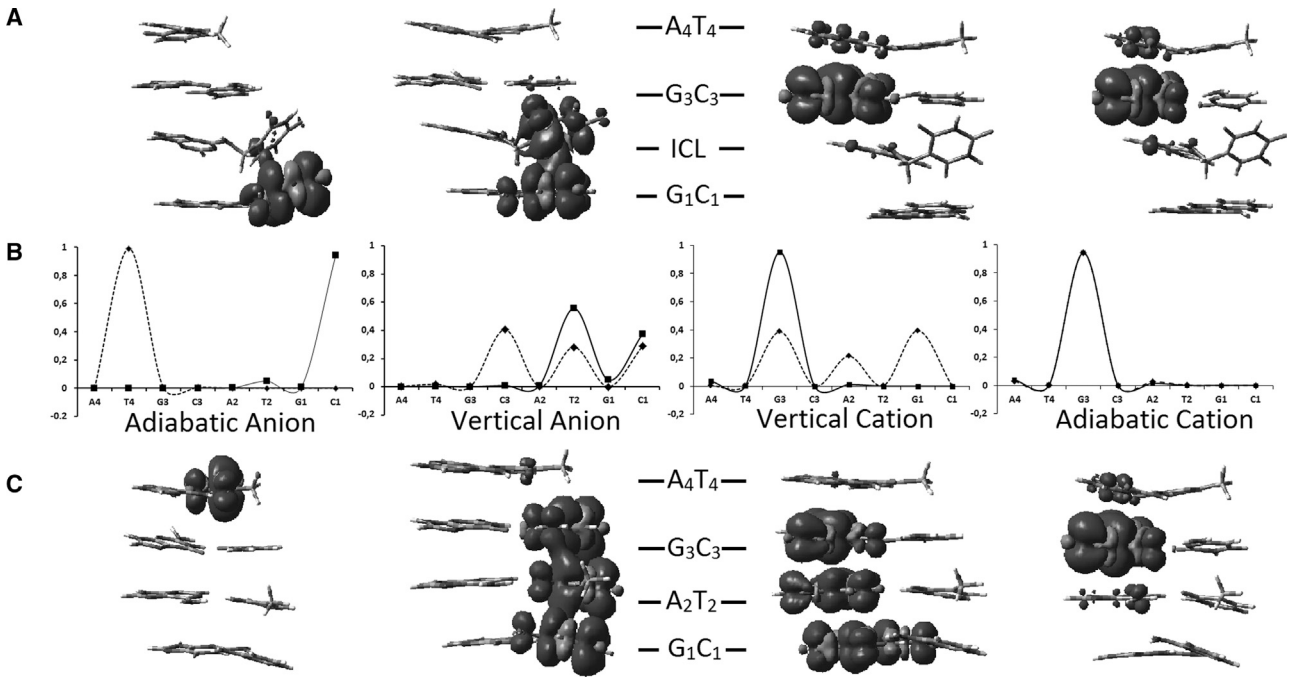


**Figure 5. Graphical Representation of dsDNA and ICL-DNA Spin Distribution**

Spin distribution in (A) cross-linked [AGA$^{ICL}$G]*[CT$^{ICL}$CT] and (C) [AGAG]*[CTCT] in their vertical or adiabatic anion and cation forms calculated on M062x/6-31+G* level of theory in aqueous phase. Graphs (B) represent the comparison of spin distribution between dsDNA (dotted line) and ICL-DNA (solid line).

analyzed base pairs the lowest VIP or AIP was found for $G_3C_3$ of native and cross-linked dsDNA as follows (in eV): 6.15/5.87 and 6.18/5.86. As expected, after spin distribution analysis, the highest adiabatic electron affinity (AEA) was found for the $A_4T_4$ pair of native dsDNA and for $G_1C_1$ of the cross-linked one, surprisingly, at the same level of 1.88 eV. The situation is much more complicated in the case of VEA; all the base and nucleoside pairs of both the discussed macromolecules adopted comparable values in a range between 1.41 and 1.53 eV. However, the higher VEA for the AT-ICL of cross-linked DNA was measured to be 1.53 eV, while in dsDNA was measured for both $G_3C_3$ and $G_1C_1$ pairs at 1.47 and 1.50 eV, respectively. These differences in the obtained electronic properties (AIP and AEA) of isolated base pairs were transferred into nuclear relaxation energy (NRE). The highest NRE was found for the base pairs that show a lower ionization potential and electron affinity, as presented in Table 3, i.e., $G_3C_3$ and $A_4T_4$, $G_1C_1$. These differences can play a significant role in charge transfer through the double helix.

### Charge Transfer through Native and Cross-Linked dsDNA

The charge migration in dsDNA can be recognized in three categories: single-step tunneling, random-walk multistep, and polaron-like hopping.[65] For the incoherent mechanism, the long charge migration between G:::C pairs is strongly dependent on the nature of the A::T pairs, which can be recognized as a bridge.[66] It has been shown experimentally that the guanine radical cation can form far from the initial place of oxidation of dsDNA, more than 200 Å away. Contrary to that is the single-step superexchange mechanism, which leads to charge migration over a short distance of around 20 Å. Therefore, multi-step thermal hopping can be recognized as an iterative single step between separate guanines, and the bridge between them, containing 1–3 AT base pairs, is usually not oxidized.[67] It is important to mention here that charge transfer through dsDNA may occur in its oxidative or reduced state. In both cases, the electronic properties of nucleobases are essential; guanosine and adenine are assigned a lower ionization potential, while pyrimidines are most easily reduced.

The most successful theory of charge transfer was introduced and developed by Marcus.[68,69] Two types of this process can be distinguished, depending on electron-coupling magnitudes, i.e., adiabatic and nonadiabatic (diabatic).[70] More details can be read in some excellent reviews.[71] As shown in Figure 6, the charge transfer depends on several factors: the structure of π-stacks and the spatial mutual position of the donor and acceptor, which determine the rate constant ($k_{ET}$), driving force $\Delta G$, reorganization (λ)/activation ($E_a$), and electron-coupling ($V_{da}$) energies. In the classical Marcus theory, the $k_{ET}$ links all the above parameters together in Equation 1, where the activation energy ($E_a$) is given by Equation 2, in which $k_b$ is the Boltzmann constant, $h$ is the Planck constant, and $T$ is temperature (K).

$$k_{ET} = \frac{4\pi |V_{da}|^2}{h} \cdot \sqrt{\frac{1}{4\pi\lambda k_b T}} \cdot \exp\left(\frac{-(\Delta G + \lambda)^2}{4\pi k_b T}\right) \quad \text{(Equation 1)}$$

**Table 3. AEA, VEA, AIP, VIP, VEAE, VEDE, and NER (in eV) and Suitable DMs of dsDNA, ICL-DNA, and Constituent Base Pair Moieties, Calculated on the m062x/6-31+G* Level of Theory in Aqueous Phase**

| | Complete ds-oligonucleotide | | Stacked Base Pair | | Base Pairs Isolated from ds-oligonucleotides | | | | | | | |
|---|---|---|---|---|---|---|---|---|---|---|---|---|
| | | | | | d[$A_4G_3A_2G_1$]*d[$C_1T_2C_3T_4$] | | | | d[$A_4G_3A_2^{ICL}G_1$]*d[$C_1T_2^{ICL}C_3T_4$] | | | |
| | dsDNA | ICL-DNA | dsDNA | ICL-DNA | $A_4T_4$ | $G_3C_3$ | $A_2T_2$ | $G_1C_1$ | $A_4T_4$ | $G_3C_3$ | $AT^{ICL}$ | $G_1C_1$ |
| $DM^{Neutral}$ | 33.74 | 42.29 | 16.33 | 11.17 | 7.69 | 10.08 | 2.43 | 5.81 | 7.21 | 8.66 | 8.91 | 4.12 |
| VEAE | 5.35 | 5.37 | 4.97 | 5.00 | 6.57 | 5.51 | 6.56 | 6.10 | 6.58 | 5.50 | 6.62 | 6.19 |
| $DM^{VEAE}$ | 35.57 | 45.65 | 19.25 | 14.14 | 6.76 | 5.50 | 3.03 | 12.29 | 7.31 | 11.92 | 9.69 | 4.34 |
| VEDE | −2.43 | −2.44 | −1.83 | −2.02 | −2.27 | −1.46 | −1.44 | −1.52 | −1.47 | −1.52 | 1.64 | −2.21 |
| $DM^{VEDE}$ | 37.25 | 41.51 | 18.97 | 12.87 | 9.56 | 9.45 | 2.34 | 5.56 | 8.23 | 9.85 | 9.99 | 8.37 |
| VIP | 6.32 | 6.15 | 5.95 | 5.83 | 6.60 | 6.15 | 6.60 | 6.15 | 6.58 | 6.18 | 6.57 | 6.19 |
| $DM^{VIP}$ | 30.65 | 34.67 | 12.60 | 8.83 | 7.51 | 2.99 | 11.01 | 8.54 | 21.88 | 4.19 | 14.13 | 9.24 |
| AIP | 5.67 | 5.71 | 5.33 | 5.35 | 6.57 | 5.87 | 6.57 | 6.11 | 6.58 | 5.86 | 6.64 | 6.19 |
| $DM^{AIP}$ | 24.23 | 35.56 | 11.09 | 7.66 | 7.55 | 2.24 | 10.59 | 8.31 | 7.18 | 2.33 | 15.06 | 9.14 |
| VEA | 1.55 | 1.49 | 0.76 | 0.97 | 1.44 | 1.47 | 1.41 | 1.50 | 1.43 | 1.49 | 1.53 | 1.46 |
| $DM^{VEA}$ | 31.46 | 57.52 | 5.98 | 18.61 | 14.08 | 15.47 | 17.80 | 18.99 | 14.06 | 14.64 | 24.25 | 18.78 |
| AEA | 1.64 | 1.91 | 1.02 | 1.39 | 1.88 | 1.42 | 1.44 | 1.54 | 1.46 | 1.54 | 1.63 | 1.88 |
| $DM^{AEA}$ | 36.52 | 63.60 | 27.63 | 27.55 | 11.10 | 15.22 | 17.66 | 19.27 | 13.69 | 15.41 | 25.65 | 19.01 |
| NER1 | 0.66 | 0.45 | 0.62 | 0.48 | 0.03 | 0.28 | 0.04 | 0.03 | 0.00 | 0.32 | −0.07 | 0.00 |
| NER2 | 0.31 | 0.34 | 0.36 | 0.35 | 0.00 | 0.37 | 0.00 | 0.02 | 0.00 | 0.36 | 0.02 | 0.00 |
| NER3 | 0.09 | 0.41 | 0.26 | 0.42 | 0.44 | −0.04 | 0.03 | 0.03 | 0.03 | 0.05 | 0.10 | 0.42 |
| NER4 | 0.79 | 0.53 | 0.81 | 0.63 | 0.39 | 0.03 | −0.01 | −0.02 | 0.00 | −0.02 | 0.01 | 0.34 |

AEA, adiabatic electron affinity; VEA, vertical electron affinity; AIP, adiabatic ionization potential; VIP, vertical ionization potential; VEAE, vertical electro attachment energy; VEDE, vertical electro detachment energy; NER, nuclear relaxation energy; DM, dipole moment.

$$E_a = \frac{\lambda}{4}\cdot\left(1+\frac{\Delta G}{\lambda}\right)^2 \qquad \text{(Equation 2)}$$

Therefore, the rate of charge transfer was influenced by electron coupling, which depends not only on the distance between donor and acceptor but also on the energy gap. These parameters can be calculated using several methods.[71] In these studies, the $V_{da}$ was calculated according to the GMH (generalized Mulliken-Hush) method, based on the acceptor-donor diabatic transition DM and vertical excitation energy of radical cation or radical anion $\Delta E_{12}$ (Equation 3).[72,73] Here $\mu_1 - \mu_2$ is the difference between the ground and first excited DM, and $\mu_{12}$ is the transition DM.

$$V_{da} = \frac{\Delta E_{12}|\mu_{12}|}{\sqrt{(\mu_1-\mu_2)^2+4\mu_{12}^2}} \qquad \text{(Equation 3)}$$

Within the terms of the occupied Kohn-Sham orbital method, the $\Delta E_{12}$ of a radical cation and anion can be estimated as the difference in energy, i.e., $\Delta E_{12} = \varepsilon_{HOMO} - \varepsilon_{HOMO-1}$ and $\Delta E_{12} = \varepsilon_{LUMO} - \varepsilon_{LUMO+1}$, respectively, calculated for neutral stacks.[74,75]

Due to the nature of charge transfer, which passes through vertical states of donor and acceptor, the most important parameter is the reorganization energy, which is associated with the movement of internal geometries and changes in the polarization environment.[76] The free energy difference between the initial and final states of charge transfer is known as the process driving force ($\Delta G$). This parameter is in fact the difference in redox potential of the investigated system, which indirectly induces Equation 1, the adiabatic and vertical electronic parameters of nucleobases or base pairs. Therefore, as per Voityuk, "the energy for charge transfer between two nucleobases can be estimated as the difference of ionization energies or electron affinity of these bases embedded in the duplex."[67] Systematic studies in this field have been performed by Saito.[77] As shown above, the charge transfer can occur in oxidized and reduced ds-oligonucleotides. Therefore, the electron or hole moves through neighboring stacked base pairs. On the other hand, it is known that the radical cation transfer occurs between guanines separated by n-AT pairs (a bridge). The analysis of ionization potential of base G involved in different triplets denoted as 5′-XGY showed that guanines on the 5′ end adopt a lower IP value *in vitro*.[78] Additionally, inspection of all the possible trimers indicated that the ability of the central base pair to lose an electron is strongly affected by the nature of the 3′ end base pair.[79,80] As shown in Table 3, the 5′ end-located guanosine adopts lower IP values in both lesioned (5.86 eV) and undamaged DNA (5.87 eV). Due to the neglected differences, it can be expected that the mechanism of hole transfer in the discussed dsDNAs should be the same. However, the different HOMO localization and spin

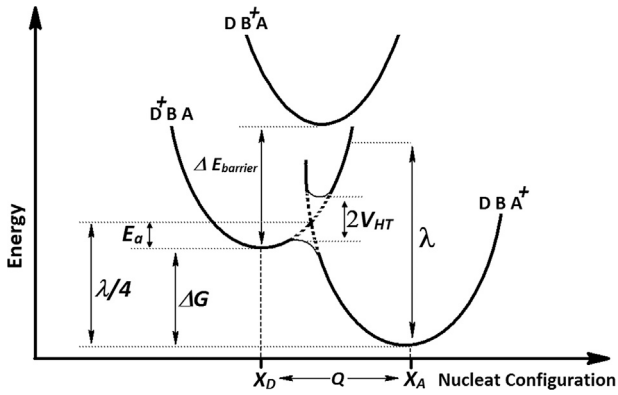


**Figure 6. The Scheme of Energy Changes in the Hole Transfer Process**
The free energy profile of hole transfer between base pairs denoted as donor (D) and acceptor (A) intervening by bridge (B) base pair.

distribution in the vertical cation state suggest a significant role of the AT-ICL in these process (Figures 4 and 5).

Therefore, first the energy barriers in vertical and adiabatic modes of charge migration were estimated. In these studies, the investigated tetramers were divided into two trimers (notification has been simplified to the base sequence of purine strand, i.e., $G_1A_2G_3$ and $A_2G_3A_4$ or $G_1ICL_2G_3$ and $ICLG_3A_4$. Therefore, the following energy barriers of radical cation transfer can be assigned: $G_1^+X_2G_3 \rightarrow G_1X_2^+G_3$ and $A_2X_3^+A_4 \rightarrow A_2X_3A_4^+$ (X = A or A-ICL) (Figure 7). Following the nature of the charge migration process, the energies of the donor and acceptor were described as the sum of the energies of suitable base pairs, extracted from an adequate tetramer, for example, the energy of donor $G_1(E_+^+)$, $X_2(E_0^0)$, $G_3(E_0^0)$ and acceptor $G_1(E_0^0)$, $X_2(E_+^0)$, $G_3(E_+^+)$. The energy barrier (base pair system) was described as the sum of $G_1(E_+^0)$, $X_2(E_0^+)$, $G_3(E_0^0)$ energies in the vertical or $G_1(E_+^0)$, $X_2(E_+^+)$, $G_3(E_0^0)$ in the adiabatic mode. The barriers 0.47/0.51 and 0.45/37 eV for $G_1 \rightarrow A_2$ and $G_1 \rightarrow$ ICL charge transfer in adiabatic/vertical mode, respectively, were found. Moreover, the barrier for the $G_3 \rightarrow A_4$ hole migration was found to be almost two times higher than previously in the vertical mode, i.e., 0.81 and 0.74 eV for the $A_2G_3A_4$ and $ICLG_3A_4$ systems, respectively. On the other hand, i.e., the adiabatic approach, these values were measured as follows: 0.72 and 0.68 eV. These data clearly indicated that the presence of the AT-ICL in the structure of a double helix did not significantly affect the barrier for hole transfer. Moreover, for the investigated systems, the $G_3C_3$ base pair served the role of a charge trap, where energy lies in the valley surrounded by barrier hills. These results are in good agreement with experimental data, which indicated that 5′ end guanine or, for example, 8-oxo-dG with lower ionization potential, serves the role of charge trapping or recombination.[48]

The analysis of both charge and spin distribution and orbital localization show that the presence of the AT-ICL forces a significant influence on electron transfer in dsDNA. Using a similar strategy as above, the barrier of excess electron transfer through the double helix was assigned. The short ds-oligonucleotides were divided into two trimers for which the energies of the electron donor, acceptor, and barrier were calculated (X = AT or ICL): (1) $G_1X_2G_3$: $G_1(E_-^-)$, $X_2(E_0^0)$, $G_3(E_0^0)$; $G_1(E_0^0)$, $X_2(E_-^0)$, $G_3(E_-^-)$; and $G_1(E_-^0)$, $X_2(E_0^-)$, $G_3(E_0^0)$ vertical or adiabatic mode $G_1(E_-^0)$, $X_2(E_-^-)$, $G_3(E_0^0)$; (2) $X_2G_3A_4$: $X_2(E_-^-)$, $G_3(E_0^0)$, $A_4(E_0^0)$; $X_2(E_0^0)$, $G_3(E_-^0)$, $A_4(E_-^-)$; and $X_2(E_-^0)$, $G_3(E_0^-)$, $A_4(E_0^0)$ vertical or adiabatic approach $X_2(E_-^0)$, $G_3(E_-^-)$, $A_4(E_0^0)$. The following barriers of electron transfer were found for native and cross-linked ds-trimers $G_1X_2G_3$ (X = AT or ICL): 0.07/0.11 eV of $G_1 \rightarrow A_2$ and 0.58/0.68 eV of $G_1 \rightarrow$ ICL in the adiabatic and vertical modes, respectively. Surprisingly, no barriers were found in the case of the $A_2G_3A_4$ electron transfer $A_2 \rightarrow G_3$ and $G_3 \rightarrow A_4$ as well as for $A_2 \rightarrow G_3$ in the case of $G_1A_2G_3$. The listed steps of charge migration processes adopted the following values (eV), namely, 0.03/−0.04, −0.41/0.07, and 0.01/−0.03, respectively (adiabatic/vertical mode). It is indicated that the electron migrated from the $G_1C_1$ base pair to $A_4T_4$ through the $[A_2G_3]^*[C_3T_2]$ part. Moreover, as has been shown, this process is privileged instead of that in the opposite direction.

The AT cross-link appearing in the structure of the double helix led to different results: first, the energy barrier for $G_1 \rightarrow$ ICL transfer was around ten times higher than that assigned for undamaged dsDNA; second, $G_1(E_-^-)$ $ICL(E_0^0)$ $G_3(E_0^0)$ adopted the lowest value in the discussed system; and, third, the electron transfer in the case of the ICL $G_3A_4$ system adopted a positive value (adiabatic/vertical), i.e., 0.10/0.15 eV for ICL $\rightarrow G_3$ and 0.05/0.03 eV for $G_3 \rightarrow A_4$, when the transfer was examined in the ICL to $A_4T_4$ direction. Due to the above, the AT-ICL constituted a stop point or significant barrier for electron transfer in dsDNA. Moreover, the spin and charge in ICL-DNA accumulated on the $G_1C_1$ pair instead of $A_4T_4$ in unmodified dsDNA. Figure 7 illustrates the difference in barriers of the "hole" or excess electron migration process through an undamaged and cross-linked double helix.

As already mentioned above, the charge transfer between stacked base pairs depends on their spatial distance. According to the Standard Reference Frame for Nucleic Acids, this distance is described by the rise parameter, which adopted a significantly higher (∼1,4 Å) value for the $[A_2T_2]^*[G_1C_1]$ base pairs of ICL-DNA than for those of dsDNA, while $[G_3C_3]^*[A_2T_2]$ was almost unaffected. Surprisingly, this relationship was observed for the cationic, neutral, and anionic forms of the discussed ds-oligonucleotide (Table S2). The lack of relationship between distance and energy barrier forces the analysis of distances between bases in single (isolated) strands. It should be pointed out here that the whole transfer went mainly through the purine tract, while the electron migrated along the pyrimidine tract. As shown in Table S6, the distances between purine rings were noted at the same level (the average difference is 0.18 Å) for both ds-oligonucleotides. The situation is the reverse in the case of pyrimidines, where the presence of the cross-link forces significant changes in the gap between $C_3/T_2$ and $T_2/C_1$ by an average value of 2.73 and 4.2 Å, respectively, compared to the native dsDNA. These results indicated that the presence of the AT cross-link should leave the hole transfer through

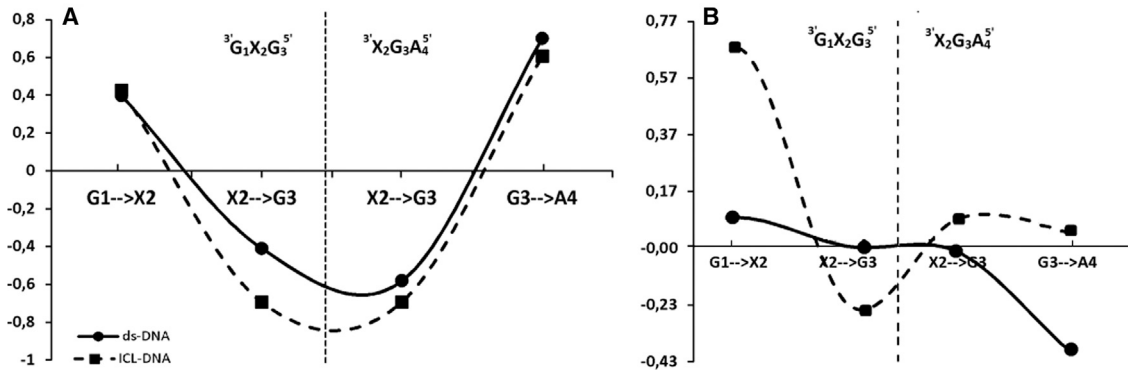


**Figure 7. Energy Barrier Profiles of the Hole and Electron Migration Process through dsDNA and ICL-DNA**

Graphical representation of energy barrier during (A) hole and (B) electron migration process through undamaged dsDNA (dotted line) and ICL-DNA (solid line), calculated on the m062x/6-31+G* level of theory in aqueous phase. $X_2$, adenine moiety of native AT base pair or AT cross-link.

the double helix almost unaffected as in native dsDNA, while the electron transfer encounters a structural obstacle in the form of rotated thymidine derived from the AT-ICL. The above outcomes are in good agreement with the energy barrier profiles presented in Figure 7.

The charge migration through stacked bases along strands of the discussed tetramer can be considered an iterative single-step superexchange process. The charge migration direction was determined by a negative Gibbs free energy of the reaction. The permitted hole or electron migrations are presented in Table 4.

The comparison of the radical cation transfer within the neighboring base pairs did not reveal a difference between ICL-DNA and native DNA. However, the hole hopping through the intervening base pair between the $[A_4T_4]^*[A_2T_2]$ and $[AT\text{-}ICL]^*[A_4T_4]$ systems revealed some differences. The presence of the AT-ICL forces a transfer from the AT-ICL to $[A_4T_4]$, while, in the case of native dsDNA, the charge migration from $[A_4T_4]$ to $[A_2T_2]$ is permitted. Surprisingly, these differences were not observed for the $[G_3C_3]^*[G_1C_1]$ system. These results are supported by the similarity in ionization potential value of the single base pairs and spin distribution of cross-linked and unmodified dsDNA (Tables 3, S5A, and S5B).

The influence of the AT-ICL's presence in the double helix on anion radical migration through a stacked system was more visible than previously. In the case of the AT-ICL, the negative charge was dispatched to the $[G_1C_1]$ location, while the unmodified adenine thymine system $[A_2T_2]$ forced the charge migration in the opposite direction of dsDNA, i.e., $[A_4T_4]$. This was shown by a spin density analysis of the ground state of the negatively charged cross-linked and native double-stranded tetramers. Moreover, these differences can derive from the uniqueness of the spin and charge distribution within the suitable vertical forms (Tables S5A and S5B; Figure 5). Additionally, this result goes well with the calculated driving force parameter ($\Delta G$). Driving force by definition is the difference of redox potentials of a donor and acceptor. For the lesioned and canonical dsDNA, the highest $|\Delta G|$ value was found, at the same level, for the radical cation migration from $A_4T_4$ to $G_3C_3$ and from $A_2T_2$ (or AT-ICL) to $G_3C_3$ (Table 4). As expected, the lowest $|\Delta G|$ values were noted for $[A_4T_4] \rightarrow [A_2T_2]$ and $[AT\text{-}ICL] \rightarrow [A_4T_4]$ hole hopping as 0.003 and 0.06 eV, respectively. For the excess electron migration through the double helix, a highest value of $|\Delta G|$ was found for the following transfers: $[A_4T_4] \rightarrow [A_2T_2]$ (0.43 eV) and $[G_3C_3] \rightarrow [G_1C_1]$ (0.11 eV) for native dsDNA and $[G_3C_3] \rightarrow [G_1C_1]$ (0.34 eV) and $[AT\text{-}ICL] \rightarrow [G_1C_1]$ (0.25 eV) for cross-linked ds-oligonucleotide.

The charge migration forced intra-molecular geometry changes to the suitable base pairs, donor ($d$) and acceptor ($a$), accompanied by reorganization energy ($\lambda$), which consists of two parts internal ($\lambda_i$) and solvent ($\lambda_s$) terms. The $\lambda_i$ describes the energy changes of adjacent structures, which occur during the hole or electron migration reaction and are represented by $\lambda_I = \lambda_1(d) + \lambda_2(a)$. In this equation, $\lambda_1(d)$ and $\lambda_2(a)$ can be calculated as follows for a hole transfer: $\lambda_1(d) = E_+^0(d) - E_0^0(d)$ and $\lambda_2(a) = E_0^+(a) - E_+^+(a)$; and for the electron transfer: $\lambda_1(d) = E_-^0(d) - E_0^0(d)$ and $\lambda_2(a) = E_0^-(a) - E_-^-(a)$. In Figure S2 they are represented by suitable NER parameters. The highest values of net reorganization energy were found for the radical cation transfer $G_1C_1 \rightarrow G_3C_3$ and $AT\text{-}ICL \rightarrow G_3C_3$ for native and cross-linked dsDNA (Table 4). Contrary to that, the lowest $\lambda_i$ was assigned for $A_4T_4 \rightarrow A_2A_2$ and $ICL \rightarrow A_4T_4$. Moreover, the lack of significant changes in the nuclear reorganization energy suggests that the hole transfer through AT base pairs is almost unaffected. This is in good agreement with the experimental data of Giese, which suggest that radical cation transfer between adenines takes place in distance-independent ways.[81]

The excess electron appearing in the system of ICL-DNA and canonical dsDNA leads to different results in reorganization energies (Table 4). In the case of native double helix, the highest $\lambda_i$ was noticed for the $G_3C_3 \rightarrow A_4T_4$ transfer, and as can be expected for $A_2T_2 \rightarrow A_4T_4$, which indicated that the$A_4T_4$ base pair is the destination of the electron transfer. The situation is different when an AT cross-link is formed in the dsDNA structure. The reorganization energies for $G_3C_3 \rightarrow G_1C_1$ (0.40 eV) and $A_4T_4 \rightarrow$ ICL (0.11 eV) were

**Table 4. The $\Delta G$, λ, $E_a$, $V_{da}$, and $K_{ET}$ of Permissible Hole and Electron Transfer between Base Pairs, Calculated on the m062x/6-31+G* Level of Theory in Aqueous Phase**

| | λ (λ$_1$+λ$_2$) (eV) | Coupling Energies (V$_{da}$) (eV) | $\Delta G$ (eV) | $E_a$ (eV) | $k_{ET}$ (s$^{-1}$) |
|---|---|---|---|---|---|
| Hole Transfer between Base Pairs | | | | | |
| [AGAG]*[CTCT] | | | | | |
| $[A_4T_4]^+[G_3C_3] \rightarrow [A_4T_4][G_3C_3]^+$ | 0.28 | 0.14 | −0.70 | 0.16 | $1.23 \times 10^{12}$ |
| $[G_3C_3][A_2T_2]^+ \rightarrow [G_3C_3]^+[A_2T_2]$ | 0.28 | 0.18 | −0.70 | 0.15 | $3.00 \times 10^{12}$ |
| $[A_2T_2]^+[G_1C_1] \rightarrow [A_2T_2][G_1C_1]^+$ | 0.04 | 0.27 | −0.46 | 1.12 | $7.15 \times 10^{-4}$ |
| $[G_3C_3][G_1C_1]^+ \rightarrow [G_3C_3]^+[G_1C_1]$ | 0.30 | 0.02 | −0.24 | 0.003 | $9.85 \times 10^{12}$ |
| $[A_4T_4]^+[A_2T_2] \rightarrow [A_4T_4][A_2T_2]^+$ | 0.04 | 0.001 | −0.003 | 0.008 | $6.15 \times 10^{10}$ |
| [AGA$^{\mathbf{ICL}}$G]*[CT$^{\mathbf{ICL}}$CT] | | | | | |
| $[A_4T_4]^+[G_3C_3] \rightarrow [A_4T_4][G_3C_3]^+$ | 0.31 | 0.21 | −0.72 | 0.13 | $8.45 \times 10^{12}$ |
| $[G_3C_3][ICL]^+ \rightarrow [G_3C_3]^+[ICL]$ | 0.34 | 0.06 | −0.77 | 0.14 | $4.46 \times 10^{11}$ |
| $[ICL]^+[G_1C_1] \rightarrow [ICL][G_1C_1]^+$ | 0.02 | 0.14 | −0.44 | 3,14 | $1.95 \times 10^{-38}$ |
| $[G_3C_3][G_1C_1]^+ \rightarrow [G_3C_3]^+[G_1C_1]$ | 0.32 | 0.003 | −0.33 | $7.86 \times 10^{-5}$ | $2.67 \times 10^{11}$ |
| $[A_4T_4][ICL]^+ \rightarrow [A_4T_4]^+[ICL]$ | 0.02 | 0.007 | −0.06 | 0.011 | $3.79 \times 10^{12}$ |
| Electron Transfer between Base Pairs | | | | | |
| d[AGAG]*d[CTCT] | | | | | |
| $[A_4T_4][G_3C_3]^- \rightarrow [A_4T_4]^-[G_3C_3]$ | 0.48 | 0.07 | −0.08 | $2 \times 10^{-4}$ | $1.17 \times 10^{14}$ |
| $[G_3C_3]^-[A_2T_2] \rightarrow [G_3C_3]\ [A_2T_2]^-$ | 0.06 | 0.05 | −0.02 | 0.007 | $1.31 \times 10^{14}$ |
| $[A_2T_2]^-[G_1C_1] \rightarrow [A_2T_2][G_1C_1]^-$ | 0.02 | 0.08 | −0.09 | 0.053 | $9.66 \times 10^{13}$ |
| $[G_3C_3]^-[G_1C_1] \rightarrow [G_3C_3][G_1C_1]^-$ | 0.06 | 0.04 | −0.11 | 0.009 | $7.73 \times 10^{13}$ |
| $[A_4T_4]\ [A_2T_2]^- \rightarrow [A_4T_4]^-[A_2T_2]$ | 0.43 | 0.05 | −0.43 | $5.2 \times 10^{-7}$ | $6.41 \times 10^{13}$ |
| d[AGA$^{\mathbf{ICL}}$G]*d[CT$^{\mathbf{ICL}}$CT] | | | | | |
| $[A_4T_4]^-[G_3C_3] \rightarrow [A_4T_4][G_3C_3]^-$ | 0.01 | 0.01 | −0.08 | 0.123 | $1,4 \times 10^{11}$ |
| $[G_3C_3]^-[ICL] \rightarrow [G_3C_3][ICL]^-$ | 0.08 | 0.02 | −0.09 | 0.003 | $2.11 \times 10^{13}$ |
| $[ICL]^-[G_1C_1] \rightarrow [ICL][G_1C_1]^-$ | 0.43 | 0.12 | −0.25 | 0.020 | $1.69 \times 10^{14}$ |
| $[G_3C_3]^-[G_1C_1] \rightarrow [G_3C_3][G_1C_1]^-$ | 0.40 | 0.03 | −0.34 | 0.003 | $2.13 \times 10^{13}$ |
| $[A_4T_4]^-[ICL] \rightarrow [A_4T_4][ICL]^-$ | 0.11 | 0.005 | −0.17 | 0.009 | $8.92 \times 10^{11}$ |

$\Delta G$, free energy; λ, nuclear relaxation energy; $E_a$, activation energy; $V_{da}$, coupling energy; $k_{ET}$, rate constant.

measured. Moreover, the electron transfer from ICL to $G_1C_1$ forced the $\lambda_i$ at a level of 0.43 eV. These observations clearly indicate that the AT-ICL disturbs the electron transfer through stacked pyrimidines, probably due to the distance perturbation between advancement systems of up to 7Å (Table S6). Therefore, the transfer in the $A_4T_4$ direction was restricted instead of the transfer in the $G_1C_1$ direction.

Figure 6 illustrates the distortion of the donor and acceptor along the charge transfer coordinates from its equilibrium to its transition state, represented graphically as an intersection of parabolas. Therefore, the charge transfer activation energy $E_a$ can be expressed as a function of the two previous parameters, i.e., λ and $\Delta G$, as shown by Equation 2. Following the Marcus theory, the hole transfer can be recognized as an isoergonic process for $\Delta G = 0$ with significant activation energy increases, for $0 \leq \Delta G \leq \lambda$ where the parabola intersections lie on the side of the normal region the maximum rate constant has been achieved for $\Delta G = \lambda$, and above this point when the $\Delta G > \lambda$ (inverted region) the reaction becomes highly exergonic; therefore, the activation energy increases with subsequent rate constant decreases.[82] The analysis of the calculated activation energies (Table 4) for the hole transfer process reveals the highest value for $A_2T_2 \rightarrow G_3C_3$ (0.15 eV) and $A_4T_4 \rightarrow G_3C_3$ (0.16 eV) for native dsDNA. Subsequently, the activation energy requirements for $A_2T_2 \rightarrow G_1C_1$ were observed as 1.12 eV.

A comparison of the above data with results obtained for the ICL-DNA revealed some similarity of $E_a$, which adopted 0.14 eV for the AT-ICL $\rightarrow G_3C_3$ transfer. On the other hand, the presence of the AT-ICL in the structure leads to significant activation energy increases of up to 3.14 eV, which indicated that the ICL becomes a dam for the hole transfer through the double helix. Alternatively, charge hopping between adenines or guanines, separated by an additional base pair, can occur. As presented in Table 4, for both the discussed oligonucleotides, a low $E_a$ for $G_1C_1 \rightarrow G_3C_3$ and $A_2T_2 \rightarrow A_4T_4$ transfer was found. It should be pointed out that the

activation energy between base pairs depends on the intervening system, as has been shown by Majima and colleagues.[83] Additionally, the changes in the double-helix structure forced by the AT-ICL led to increases in the $E_a$ by 0.03 eV versus the native AT base pair for the $A_2T_2 \rightarrow A_4T_4$ process with a subsequent decrease in the value for the $G_1C_1 \rightarrow G_3C_3$ process. The small activation energy found for the adenine-adenine charge migration is in good agreement with the experimental data of Giese.[81] Moreover, the obtained results suggest that the hole transfer of $G_1C_1 \rightarrow G_3C_3$ over the AT cross-link can occur. Additionally, the neglected geometry changes in the purine part of AT cross-link allowed $AT^{ICL} \rightarrow A_4T_4$ hole hopping at almost the same level as was found for native dsDNA (Table 4).

An analysis of the energy activation of an additional electron transfer through stacked base pairs revealed the lowest value for $G_3C_3 \rightarrow A_4T_4$ ($2 \times 10^{-4}$ eV) and through the intervening base pair $A_2T_2 \rightarrow A_4T_4$ ($5.2 \times 10^{-7}$ eV), subsequently the highest $E_a$ value was observed for $G_1C_1 \rightarrow A_2T_2$ 0.053 eV (Table 4). These results fit well with the assigned reorganization energy, which can be recognized as a factor of structural change forced by a charge transfer. It is important to mention here that the noticeable structural distortion, triggered by the extra electron attachment, was indicated by a valence type anion formation; contrary to this, the lack of spatial geometry changes accompany the dipole type anion. In the second case, the electron should be easily transferred from base to base until it settles in a favorable place, characterized by the highest electron affinity, i.e., the $A_4T_4$ base pair (AEA = 1.88 eV) of native dsDNA. The presence of the AT-ICL in the double helix forces a different pattern of activation energy values compared to native dsDNA. First of all, a moderate $E_a$ was found for the electron transfer from AT-ICL $\rightarrow G_1C_1$, 0.02 eV, which indicated the transfer through $A^{ICL}T^{ICL}$ is possible. The highest one was assigned for the $A_4T_4 \rightarrow G_3C_3$ transfer at 0.123 eV. It is not surprising because the distance between the AT-ICL and adjacent 3′/5′ pyrimidines is approximately 6.5 Å, assigned in accordance with the standard reference frame parameters (Table S6). Second, scarcely any values of $E_a$ were denoted for the $G_1C_1 \rightarrow G_3C_3$ transfer and for $G_3C_3 \rightarrow A_2T_2{}^{ICL}$. These results suggest that the negative charge through cross-linked DNA migrates in the opposite direction than in native ds-oligonucleotide, i.e., $G_1C_1$, which was characterized by the highest AEA value at 1.88 eV.

As shown in Figure 6, the $V_{da}$ is one of the most important parameters for charge transfer consideration. First, $V_{da}$ is involved in the transfer rate constant (Equation 1); moreover, it determines the dependence of $k_{ET}$ and the distance between the donor and acceptor. Additionally to that, Voityuk[84] has shown that the $V_{da}$ is strongly related to mutual acceptor and donor spatial orientation. Systematic calculation revealed that even the base pairs involved in charge transfer are separated by an intervening unit, the orbitals do not overlap significantly, and the coupling is mediated by the superexchange process. For example, $V_{da}$ = 0.082 eV was found for adjacent GG, for the separated guanines by one thymidine (GTG) $V_{da}$ decrease up to 0.008 eV.[58] Therefore, two types of discussed process can be noticed: adiabatic if $V_{da}$ adopts the moderate value ($V_{da}$~0.1) and nonadiabatic when coupling is relatively small ($V_{da} << 1$ eV).[70] It is particularly visible in the case of adjacent base pairs, where $V_{da}$ is quite high, around 0.1 eV, and its separation by even a 1-nt unit makes it several times weaker. The examination of the charge transfer process through cross-linked dsDNA revealed that the AT-ICL appearing in the structure of the double helix blunts the coupling value for the AT-ICL $\rightarrow G_3C_3$ radical cation transfer by up to 0.06 eV. Other coupling energies have been found at the same level as for unmodified ds-oligonucleotide (Table 4). It should be mentioned here that the intervening stacked base pairs by the AT-ICL lead to a decrease in $V_{da}$ by one order of magnitude in comparison to native DNA. It is indicated that the structural changes forced by a cross-link interfere with the charge migration over the double helix, and these processes become nonadiabatic for AT-ICL $\rightarrow G_3C_3$. An analysis of the other $V_{da}$ values for the rest of the adjacent stacked base pairs did not reveal significant changes between native and cross-linked DNA, leaving the hole migration process in accordance with an adiabatic regime.

The situation is much more complicated in the case of negative charge transfer. The electron-coupling energy was found to be the highest (0.12 eV) for electron migration from the AT-ICL to $G_1C_1$ base pair; additionally, the lowest (0.005 eV) value was noted for the $A_4T_4 \rightarrow$ AT-ICL electron migration. For the AT-ICL $\rightarrow G_1C_1 V_{da}$, it adopts a several times higher value than for other stacked base pairs what accompanied on a distribution of LUMO and spin density over donor and acceptor (Figures 4 and 5). Due to this, it can be concluded that the AT-ICL will constitute the stop point for electron transfer in an $A_4T_4$ direction. It can be expected that the natures of the electron transfer process through ICL-DNA and native dsDNA are different. As shown in Figures 4 and 5, the spin density in a vertical anion state as well as a LUMO in neutral state are dispersed over three base pairs, extending almost over the whole discussed tetramer. This situation is manifested by the adoption of a comparable $V_{da}$ value in the range of 0.04–0.08 eV for electron migration between all the stacked base pairs (Table 4). The obtained values for the [GC]*[AT] system are consistent with the previously calculated value of $V_{da}$ = 0.107 eV.[85]

The charge transfer rate constant $k_{ET}$ is determined by activation energy, driving force, and electronic-coupling matrix element, as expressed by Equation 3.[61] Due to the fact that $k_{ET}$ strongly depends on the distance between donor and acceptor, the influence of the AT-ICL on charge transfer in the shape of a double helix can be expected. A comparison of the allowed (negative drawing force) hole transfer rate constants of cross-linked and native dsDNA showed that the AT-ICL slowed down the radical migration from $A_2T_2 \rightarrow G_1C_1$ versus AT-ICL $\rightarrow G_1C_1$ by 34 orders of magnitude, making these transfers impossible; the following $k_{ET}$ ($s^{-1}$) were found: $7.15 \times 10^{-4}$ and $1.95 \times 10^{-38}$, respectively. The small value of $k_{ET}$ concurs well with an experimental study, which indicated that the radical cation mainly settles on G5′ from the investigated GXG trimers during hole migration.[78,80,86] Subsequently, no noticeable differences for $A_4T_4 \rightarrow G_3C_3$ were seen. The AT-ICL appearing in the system gently slowed down the radical migration by orders of magnitude between $G_1C_1 \rightarrow G_3C_3$ and AT-ICL $\rightarrow G_3C_3$, as

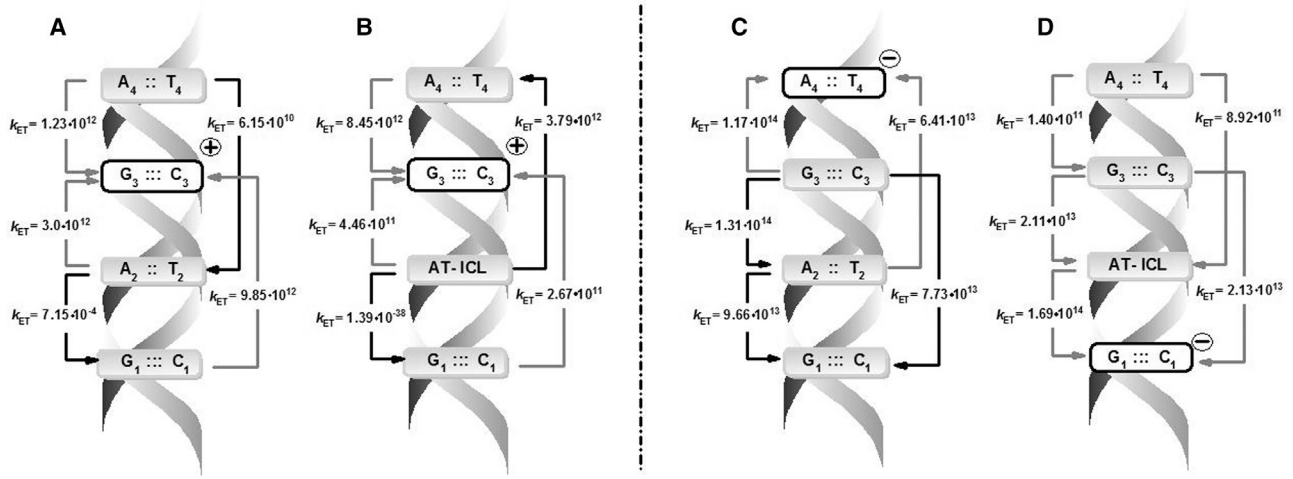


**Figure 8. Scheme of "Hole" and Electron Migration through dsDNA and ICL-DNA**

(A–D) The rate constant ($s^{-1}$) of hole and electron migration through native (A and C) and cross-linked (B and D) DNA. By arrows the directions of charge transfer are indicated (negative $\Delta G$ value of process).

presented in Table 4. These observations are in good agreement with structural and stacking analysis, which showed that the rise parameter increases, below the (3′ end), the position of the AT-ICL (Table S2) with subsequent interstrand interaction energy decreases (Table S4). A careful analysis of the positive charge migration direction revealed only one difference between the cross-linked and native dsDNA. In the case of the ICL-DNA, hole hopping between AT-ICL → $A_4T_4$ with $k_{ET} = 379 \times 10^{12}\ s^{-1}$ was noted, while for dsDNA the opposite direction was observed, $A_4T_4 \rightarrow A_2T_2$ with a smaller rate constant $6.15 \times 10^{10}\ s^{-1}$. This difference can be supported by the fact that the distance between the stacked base pairs in the case of dsDNA are higher than in ICL-DNA. The following values were found: 5.18 and 6.14 Å, respectively. It is well known that, with space increases, the rate constant of charge transfer process decreases.[85] The graphical representations of the allowed (negative $\Delta G$) hole or electron transfer with $k_{ET}$ indication are presented in Figure 8.

The electron migration through stacked base pairs in the double helix was found to be different for dsDNA and ICL-DNA. This conclusion is partly supported by the spin and charge localization, which had different places of localization (Tables S5A and S5B). The appearance of the AT-ICL in the system forces the direction of radical anion migration toward the $G_1C_1$ pair in a non-disturbing manner, while in the case of native DNA it is a more complicated process, as illustrated in Figure 8. The following orders of rate constant for electron transfer within ICL-DNA were found: $A_4T_4 \rightarrow G_3C_3 < A_4T_4 \rightarrow$ AT-ICL $<$ $G_3C_3 \rightarrow$ AT-ICL $<$ $G_3C_3 \rightarrow G_1C_1 <$ AT-ICL $\rightarrow G_1C_1$. The highest value was found for AT-ICL → $G_1C_1$ ($1.69 \times 1014\ s^{-1}$). It is quite a surprise, given the large distance between $T^{ICL}$ and $C_1$, i.e., 6.97 Å. This indicates some participation of transfer through pyrimidines: the distance between $A^{ICL}$ and $G_1$ is almost unaffected in comparison to native dsDNA (3.16 versus 3.18 Å) (Table S6). A comparative analysis of the electron transfer rate constant between dsDNA and ICL-DNA revealed that the AT-ICL slowed down the process toward the $A_4T_4$ base pair by one or two orders of magnitude (Table 4). Moreover, in the case of electron migration through dsDNA, the lower value of $E_a$ accompanies the highest $k_{ET}$, which was assigned for the $G_3C_1 \rightarrow A_4T_4$ and $A_2T_2 \rightarrow A_4T_4$ negative charge transfer while in ICL-DNA for AT-CL → $G_1C_1$. Taking all the above into consideration, it can be concluded that the spatial disorder forced by an additional covalent bond between adenine and complementary thymine changes the direction of electron migration and likewise slows down this process.

### Final Remarks and Future Studies

The main idea of QM/MM in these studies was to obtain the whole 3D structure of short dsDNA. The UFF force field was used to describe the highly malleable sugar phosphate backbone, which keeps the double helix in its proper shape, especially in the presence of a cross-link or other DNA lesions. As described above, the internal part, i.e., the stacked base pairs, was described at the M06-2x/6-31+G* level of theory. However, for a more reasonable description of the ICL influence in its physiological condition on the 3D dsDNA, molecular dynamics (MD) studies are required, even though the QM/MM optimizations were obtained at default temperature 298.15K in the condensed phase.[87] Therefore, the results of MD studies will be valuable for a cross-linked DNA structure description and its comparison to native ds-oligonucleotide.[88,89]

The presented results describe the short oligo-tetramer d[AGAG]*d[CTCT], but due to its low thermal stability ($T_m$ below 12°C) is not suitable for a full MD simulation.[90] Due to this limitation, future studies should be made for at least a decamer (assuming a reasonable calculation time) to obtain valuable results. The melting temperature of decamers is around 30°C and depends on the base sequence. Moreover, comprehensive QM/MM MD studies of different types of

intrastrand cross-link, described in the Introduction, are particularly necessary, not only in the case of spatial geometry, ground, and electronically excited state analyses but also in the case of the discussed AT-ICL formation.[6,8] The latter point is very interesting from the perspective of bioorganic chemistry as well as from chemotherapeutic activity, due to the mechanism of the Dimroth-like rearmament (see Figure 2). For this purpose, the strategy of mixed QM/MM MD simulations should be applied. This methodology has been well justified by the works of Rothlisberger, Monari, and Tuñón.[91–93] For further information, please refer to Brunk and Rothlisberger[94] and the citations there that focus its usefulness for different types of study, e.g., enzymatic reactions and capturing systems containing transition metal ions, photoactive biological chromophores, etc. Additionally, to obtain highly accurate results, the newly discovered force field for MD should be implemented, i.e., OL15 or parm99bsc1, which would avoid unexpected changes in the sugar phosphate backbone structure (e.g., spontaneous adoption *trans* conformation by the 5′OH group instead of *gauche (-)*).[95,96]

To check the legitimacy of the above, preliminary studies of an MD simulation were performed using the evaluation version of HyperChem 8.0 software for the structure discussed in the article (the negative charge of the phosphate group was quenched by $Na^+$).[97] The MD for dsDNA as well as ICL-DNA were performed using the AMBER94 force field (which is implemented in the software), a solvated box (35/25/35Å) with a TPI3P water model, at a constant temperature of 300K and pressure of 1 atm, and an MD time of 30 ps with a time step of 1 fs.[98–100]

The internal tightening present in the dsDNA containing an ICL forces a different potential energy change profile as well as their root-mean-square (RMS) deviation from the mean for adequate energy (D EPOT) during the MD studies in the solvated box (Figure S8) below the dsDNA red line, ICL-DNA blue line.[101] These observations, even for a short oligo (tetramer), indicate the significant influence of the ICL on the double helix's stability, and they justify future attempts at QM/MM MD studies.

### Conclusions

A number of DNA lessons can occur in genomic DNA as a result of environmental factor, either as unwanted by-products of cellular metabolic processes or as a product of radiotherapy or chemotherapy. One of the most harmful, in terms of cell survival, is an ICL. As shown, 40 cross-link events are lethal for *E.coli*. These unusual tandem lesions can lead to different spatial geometry changes in the double helix depending on the initial agents.

In this study, the geometries and properties of short double-stranded oligonucleotides containing AT ICL were taken into DFT theoretical consideration at the M062X/6-31+G* level of theory in the aqueous phase and a QM/MM study.

The preliminary results showed that covalent linkage (C5-N6) between adenine and thymine moieties force the structural bending of the formed AT ICL (Figure 3), leaving the electronic properties almost unaffected in comparison to the native d[A]*d[T] pair. The situation changed when the AT-ICL was located in the space of the double helix. A flattening of the AT-ICL geometry was observed due to the stacking interaction with the neighboring 5′/3′ end base pairs. The intermolecular tension was exclusively compensated by a 2′-deoxyribose ring of thymine moiety, which adopted the conformation $_2$T4. These changes with subsequent *syn* conformation of the dT unit led to rise parameter increases between the AT-ICL and adjacent base pairs. Significant distance increases between bases were noted for the pyrimidine strand, while the purine strand was almost unaffected. Surprisingly, the AT-ICL disrupted the shape of double-helix DNA less visibly than expected under a preliminary study.

This indicates that the electronic and structural properties of DNA damage should be theoretically considered as part of a double helix and not as a single isolated entity.

The electronic property consideration did not show noticeable differences between cross-linked and native dsDNA in the case of ionization potential for both macromolecules, with the $G_3C_3$ base pair adopting the lower value. Contrary to that, the $A_4T_4$ of dsDNA and $G_1C_1$ of ICL-DNA showed a higher electron affinity value. These results were consistent with Hirshfeld charge and spin distribution.

Finally, the influence of the AT-ICL on charge transfer through the double helix was considered. The obtained results indicated that the AT cross-link did not upset the hole transfer in comparison to native dsDNA; however, the rate constant for AT-ICL → $G_1C_1$ was significantly smaller than for the native $A_2T_2$ → $G_1C_1$. The much more visible effect of the AT-ICL's presence was observed for the electron transfer, i.e., first the cross-link effectively slowed down these processes in the $A_4T_4$ helix direction by order of magnitude, second the cross-link forced the direction of electron migration to the $G_1C_1$ base pair instead of $A_4T_4$, which was the destination for dsDNA.

Taking all of the above into consideration, it can be concluded that the appearance of the AT-ICL in the space of a double helix does not upset its spatial geometry significantly; however, the cross-link can have a significant meaning for charge transfer and for further DNA lesion formations.

## MATERIALS AND METHODS

### Computation Methodology of QM/MM Studies

The geometry optimizations of ds-pentamers, i.e., d[AGA$^{ICL}$G]*d[TCT$^{ICL}$C] and d[AGAG]*d[TCTC], were performed by the QM/MM strategy.[102,103] The structures of the mentioned systems were divided into high (HL) (nucleobases, M06-2X/6-31+G(d)) and low (LL) (sugar phosphate backbone, UFF) levels (layers) of calculation using the ONIOM (Our own N-layered Integrated Molecular Orbital and Molecular Mechanics) method.[104,105] Due to the complexity of the system, which contained 158 heavy atoms and 102 hydrogens, the negative charges of phosphate groups were neutralized by the addition of protons rather than positive ions like $Na^+$. This strategy has been well documented as applicable to

charge or proton transfer or structural studies of nucleic acids.[106,107] Also relevant here are the studies of Leszczynski,[108] who adopted the above strategy for low electron migration from the base moiety to the sugar phosphate backbone. Moreover, the changes of $Na^+$ to protons make the QM/MM calculation less time consuming (and therefore less expensive), especially when the calculations were performed in the condensed phase.

The obtained nucleotide complexes (ds-pentamers) were converted to nucleobase pairs, which were used for inter- and intrastrand interaction energy calculations among others. The sugar phosphate backbone was removed from the obtained structures, leaving suitable base pair systems with subsequent atom saturation with the necessary hydrogen atoms. These hydrogen atoms added for saturation were optimized at the M06-2X/6-31+G* level of theory in the aqueous phase, with the position of all other atoms fixed.

#### Computation Methodology of DFT Study

All energy calculations were performed in the aqueous phase by DFT using the M06-2X functional with augmented polarized valence double-ζ basis set 6-31+G(d).[34,109] The characterization of the transition DM of excited states and the single-point calculation at the M06-2X/6-31+G(d) level of theory were performed using time-dependent DFT (TD-DFT) methodology.[110] The solvent effect was described for an aqueous medium, applying Tomasi's PCM.[111] For all optimized structures, a charge and spin analysis was achieved using Hirshfeld methodology at the M06-2X/6-31+G(d) level.[112] The electron coupling was calculated using Generalized Mulliken-Hush methodology.[73] The electronic properties of molecules were calculated as follows:[31] AEA was obtained as the difference between the energies of the neutral and anion corresponding forms at their optimized geometries, AEA = $E_{neutral}(E_0^{\ 0}) - E_{anion}(E_-^{\ -})$; VEA was obtained as the difference between the energies of neutral and anion forms at the optimized neutral geometries, VEA = $E_{neutral}(E_0^{\ 0}) - E_{anion}(E_0^{\ -})$; vertical electron detachment energy (VEDE) was obtained as the difference between the energies of the neutral and anion forms at the optimized anion geometries, VEDE = $E_{anion}(E_-^{\ -}) - E_{neutral}(E_-^{\ 0})$; the AIP was obtained as the difference between the energies of the cationic and neutral forms at their optimized geometries, AIP = $E_{cation}(E_+^{\ +}) - E_{neutral}(E_0^{\ 0})$; VIP was the difference between the energies of cation and neutral forms at the optimized neutral geometries, VIP = $E_{cation}(E_0^{\ +}) - E_{neutral}(E_0^{\ 0})$; and the vertical electron attachment energy (VEAE) was the difference between the energies of neutral and cation forms at optimized cation geometries, VEAE = $E_{cation}(E_+^{\ +}) - E_{neutral}(E_0^{\ 0})$.

All calculations were performed in the gaseous phase on Gaussian 09 (revision A.02) software package.[87]

The visualization of all the structures, as well as the creation of suitable *.pdb files, was performed using DS Visualizer software.[113]

The three-dimensional structural analyses of the mentioned ss- and dsDNAs, based on a standard reference frame, were obtained by a 3DNA software package using the web-based interface w3DNA (web 3DNA).[114]

## SUPPLEMENTAL INFORMATION

Supplemental Information includes eight figures and nine tables and can be found with this article online at https://doi.org/10.1016/j.omtn.2018.10.014.

## AUTHOR CONTRIBUTIONS

B.T.K. conceived the study, conducted and designed the theoretical experiments, and wrote the paper.

## CONFLICTS OF INTEREST

The author declares no conflicts of interest.

## ACKNOWLEDGMENTS

This study was supported by a Medical University of Lodz grant (503-31-002) and in part by PL-Grid infrastructure (Prometheus, ACC Cyfronet AGH), for which the author is grateful.

## REFERENCES

1. von Sonntag, C. (2006). Free-Radical-Induced DNA Damage and Its Repair: A Chemical Perspective (Springer-Verlag Berlin Heidelberg).
2. Khanna, K.K., and Shiloh, Y. (2009). The DNA Damage Response: Implications on Cancer Formation and Treatment (Springer Dordrecht Heidelberg London New York).
3. Sage, E., and Shikazono, N. (2017). Radiation-induced clustered DNA lesions: Repair and mutagenesis. Free Radic. Biol. Med. *107*, 125–135.
4. Cooke, M.S., Evans, M.D., Dizdaroglu, M., and Lunec, J. (2003). Oxidative DNA damage: mechanisms, mutation, and disease. FASEB J. *17*, 1195–1214.
5. Dumont, E., and Monari, A. (2015). Understanding DNA under oxidative stress and sensitization: the role of molecular modeling. Front Chem. *3*, 43.
6. Muniandy, P.A., Liu, J., Majumdar, A., Liu, S.T., and Seidman, M.M. (2010). DNA interstrand crosslink repair in mammalian cells: step by step. Crit. Rev. Biochem. Mol. Biol. *45*, 23–49.
7. McHugh, P.J., Spanswick, V.J., and Hartley, J.A. (2001). Repair of DNA interstrand crosslinks: molecular mechanisms and clinical relevance. Lancet Oncol. *2*, 483–490.
8. Deans, A.J., and West, S.C. (2011). DNA interstrand crosslink repair and cancer. Nat. Rev. Cancer *11*, 467–480.
9. Goodman, L.S., Wintrobe, M.M., Dameshek, W., Goodman, M.J., Gilman, A., and McLennan, M.T. (1946). Nitrogen mustard therapy; use of methyl-bis(beta-chloroethyl)amine hydrochloride and tris(beta-chloroethyl)amine hydrochloride for Hodgkin's disease, lymphosarcoma, leukemia and certain allied and miscellaneous disorders. J. Am. Med. Assoc. *132*, 126–132.
10. Ojwang, J.O., Grueneberg, D.A., and Loechler, E.L. (1989). Synthesis of a duplex oligonucleotide containing a nitrogen mustard interstrand DNA-DNA cross-link. Cancer Res. *49*, 6529–6537.
11. Jamieson, E.R., and Lippard, S.J. (1999). Structure, Recognition, and Processing of Cisplatin-DNA Adducts. Chem. Rev. *99*, 2467–2498.
12. Stone, M.P., Cho, Y.J., Huang, H., Kim, H.Y., Kozekov, I.D., Kozekova, A., Wang, H., Minko, I.G., Lloyd, R.S., Harris, T.M., and Rizzo, C.J. (2008). Interstrand DNA cross-links induced by α,β-unsaturated aldehydes derived from lipid peroxidation and environmental sources. Acc. Chem. Res. *41*, 793–804.
13. Garaycoechea, J.I., Crossan, G.P., Langevin, F., Daly, M., Arends, M.J., and Patel, K.J. (2012). Genotoxic consequences of endogenous aldehydes on mouse haematopoietic stem cell function. Nature *489*, 571–575.

14. Shapiro, R., Dubelman, S., Feinberg, A.M., Crain, P.F., and McCloskey, J.A. (1977). Isolation and identification of cross-linked nucleosides from nitrous acid treated deoxyribonucleic acid. J. Am. Chem. Soc. *99*, 302–303.

15. Harwood, E.A., Hopkins, P.B., and Sigurdsson, S.T. (2000). Chemical synthesis of cross-link lesions found in nitrous acid treated DNA: a general method for the preparation of N2-substituted 2′-deoxyguanosines. J. Org. Chem. *65*, 2959–2964.

16. Guan, L., and Greenberg, M.M. (2009). DNA interstrand cross-link formation by the 1,4-dioxobutane abasic lesion. J. Am. Chem. Soc. *131*, 15225–15231.

17. Höglund, E., Blomquist, E., Carlsson, J., and Stenerlöw, B. (2000). DNA damage induced by radiation of different linear energy transfer: initial fragmentation. Int. J. Radiat. Biol. *76*, 539–547.

18. Hada, M., and Georgakilas, A.G. (2008). Formation of clustered DNA damage after high-LET irradiation: a review. J. Radiat. Res. (Tokyo) *49*, 203–210.

19. Price, N.E., Johnson, K.M., Wang, J., Fekry, M.I., Wang, Y., and Gates, K.S. (2014). Interstrand DNA-DNA cross-link formation between adenine residues and abasic sites in duplex DNA. J. Am. Chem. Soc. *136*, 3483–3490.

20. Ghosh, A., Joy, A., Schuster, G.B., Douki, T., and Cadet, J. (2008). Selective one-electron oxidation of duplex DNA oligomers: reaction at thymines. Org. Biomol. Chem. *6*, 916–928.

21. Ghosh, A.K., and Schuster, G.B. (2006). Role of the guanine N1 imino proton in the migration and reaction of radical cations in DNA oligomers. J. Am. Chem. Soc. *128*, 4172–4173.

22. Ding, H., Majumdar, A., Tolman, J.R., and Greenberg, M.M. (2008). Multinuclear NMR and kinetic analysis of DNA interstrand cross-link formation. J. Am. Chem. Soc. *130*, 17981–17987.

23. Wagenknecht, H.-A. (2006). Charge Transfer in DNA: From Mechanism to Application (Wiley-VCH Verlag).

24. Hong, I.S., and Greenberg, M.M. (2004). Mild generation of 5-(2′-deoxyuridinyl) methyl radical from a phenyl selenide precursor. Org. Lett. *6*, 5011–5013.

25. Mennucci, B., Tomasi, J., Cammi, R., Cheeseman, J.R., Frisch, M.J., Devlin, F.J., Gabriel, S., and Stephens, P.J. (2002). Polarizable continuum model (PCM) calculations of solvent effects on optical rotations of chiral molecules. J. Phys. Chem. A *106*, 6102–6113.

26. Albiser, G., Lamiri, A., and Premilat, S. (2001). The A–B transition: temperature and base composition effects on hydration of DNA. Int. J. Biol. Macromol. *28*, 199–203.

27. Karwowski, B.T. (2013). The role of (5′*R*) and (5′*S*) 5′,8-cyclo-2′-deoxyadenosine in *ds*-DNA structure: a comparative QM/MM theoretical study. Comput. Theor. Chem. *1010*, 38–44.

28. Saenger, W. (1984). Principles of Nucleic Acid Structure (Springer-Verlag New York).

29. Levitt, M., and Warshel, A. (1978). Extreme conformational flexibility of the furanose ring in DNA and RNA. J. Am. Chem. Soc. *100*, 2607–2613.

30. Altona, C., and Sundaralingam, M. (1972). Conformational analysis of the sugar ring in nucleosides and nucleotides. A new description using the concept of pseudorotation. J. Am. Chem. Soc. *94*, 8205–8212.

31. Karwowski, B.T. (2015). The influence of phosphorothioate on charge migration in single and double stranded DNA: a theoretical approach. Phys. Chem. Chem. Phys. *17*, 21507–21516.

32. Li, X., and Sevilla, M.D. (2007). DFT treatment of radiation produced radicals in DNA model systems. In Advances in Quantum Chemistry: Theory of the Interaction of Radiation with Biomolecules, Volume 52 (Academic Press), pp. 59–87.

33. Robertazzi, A., and Platts, J.A. (2006). Gas-phase DNA oligonucleotide structures. A QM/MM and atoms in molecules study. J. Phys. Chem. A *110*, 3992–4000.

34. Zhao, Y., Pu, J., Lynch, B.J., and Truhlar, D.G. (2004). Tests of second-generation and third-generation density functionals for thermochemical kinetics. Phys. Chem. Chem. Phys. *6*, 673–676.

35. Zhao, Y., and Truhlar, D.G. (2005). Design of density functionals that are broadly accurate for thermochemistry, thermochemical kinetics, and nonbonded interactions. J. Phys. Chem. A *109*, 5656–5667.

36. Rienstra-Kiracofe, J.C., Tschumper, G.S., Schaefer, H.F., 3rd, Nandi, S., and Ellison, G.B. (2002). Atomic and molecular electron affinities: photoelectron experiments and theoretical computations. Chem. Rev. *102*, 231–282.

37. Oyler, N.A., and Adamowicz, L. (1993). Electron attachment to uracil: theoretical ab initio study. J. Phys. Chem. *97*, 11122–11123.

38. Oyler, N.A., and Adamowicz, L. (1994). Theoretical ab initio calculations of the electron affinity of thymine. Chem. Phys. Lett. *219*, 223–227.

39. Roehrig, G.H., Oyler, N.A., and Adamowicz, L. (1994). Can electron attachment alter tautomeric equilibrium of guanine? Theoretical ab initio study. Chem. Phys. Lett. *225*, 265–272.

40. Watson, J.D., and Crick, F.H. (1953). Molecular structure of nucleic acids; a structure for deoxyribose nucleic acid. Nature *171*, 737–738.

41. Yakovchuk, P., Protozanova, E., and Frank-Kamenetskii, M.D. (2006). Base-stacking and base-pairing contributions into thermal stability of the DNA double helix. Nucleic Acids Res. *34*, 564–574.

42. Olson, W.K., Bansal, M., Burley, S.K., Dickerson, R.E., Gerstein, M., Harvey, S.C., Heinemann, U., Lu, X.J., Neidle, S., Shakked, Z., et al. (2001). A standard reference frame for the description of nucleic acid base-pair geometry. J. Mol. Biol. *313*, 229–237.

43. Fujita, S., Takenaka, A., and Sasada, Y. (1984). A model for interactions of amino acid side chains with Watson-Crick base pair of guanine and cytosine. Crystal structures of 9-(2-carboxyethyl)guanine and its crystalline complex with 1-methylcytosine. Bull. Chem. Soc. Jpn. *57*, 1707–1712.

44. Chakraborty, R., and Ghosh, D. (2016). The effect of sequence on the ionization of guanine in DNA. Phys. Chem. Chem. Phys. *18*, 6526–6533.

45. Di Felice, R., and Porath, D. (2008). DNA-based nanoelectronics. In NanoBioTechonology: BioInspired Devices and Materials of the Future, O. Shoseyov and I. Levy, eds. (Totowa, NJ, USA: Humana Press), pp. 141–185.

46. Genereux, J.C., and Barton, J.K. (2010). Mechanisms for DNA charge transport. Chem. Rev. *110*, 1642–1662.

47. Côté, R. (2016). Chapter Two - Ultracold Hybrid Atom–Ion Systems. Adv. At. Mol. Opt. Phys. *65*, 67–126.

48. Kanvah, S., Joseph, J., Schuster, G.B., Barnett, R.N., Cleveland, C.L., and Landman, U. (2010). Oxidation of DNA: damage to nucleobases. Acc. Chem. Res. *43*, 280–287.

49. Huang, H., Das, R.S., Basu, A.K., and Stone, M.P. (2011). Structure of (5′S)-8,5′-cyclo-2′-deoxyguanosine in DNA. J. Am. Chem. Soc. *133*, 20357–20368.

50. Karwowski, B.T., Bellon, S., O'Neill, P., Lomax, M.E., and Cadet, J. (2014). Effects of (5′S)-5′,8-cyclo-2′-deoxyadenosine on the base excision repair of oxidatively generated clustered DNA damage. A biochemical and theoretical study. Org. Biomol. Chem. *12*, 8671–8682.

51. Pande, P., Das, R.S., Sheppard, C., Kow, Y.W., and Basu, A.K. (2012). Repair efficiency of (5′S)-8,5′-cyclo-2′-deoxyguanosine and (5′S)-8,5′-cyclo-2′-deoxyadenosine depends on the complementary base. DNA Repair (Amst.) *11*, 926–931.

52. Protozanova, E., Yakovchuk, P., and Frank-Kamenetskii, M.D. (2004). Stacked-unstacked equilibrium at the nick site of DNA. J. Mol. Biol. *342*, 775–785.

53. Rooman, M., and Wintjens, R. (2014). Sequence and conformation effects on ionization potential and charge distribution of homo-nucleobase stacks using M06-2X hybrid density functional theory calculations. J. Biomol. Struct. Dyn. *32*, 532–545.

54. Mardirossian, N., and Head-Gordon, M. (2016). How Accurate Are the Minnesota Density Functionals for Noncovalent Interactions, Isomerization Energies, Thermochemistry, and Barrier Heights Involving Molecules Composed of Main-Group Elements? J. Chem. Theory Comput. *12*, 4303–4325.

55. Apalkov, V., and Chakraborty, T. (2006). Electronic properties of guanine traps in DNA. Phys. Rev. B Condens. Matter Mater. Phys. *73*, 1131031–1131034.

56. Gu, J., Leszczynski, J., and Schaefer, H.F., 3rd (2012). Interactions of electrons with bare and hydrated biomolecules: from nucleic acid bases to DNA segments. Chem. Rev. *112*, 5603–5640.

57. Venkatramani, R., Keinan, S., Balaeff, A., and Beratan, D.N. (2011). Nucleic Acid Charge Transfer: Black, White and Gray. Coord. Chem. Rev. *255*, 635–648.

58. Félix, M., and Voityuk, A.A. (2011). DFT performance for the hole transfer parameters in DNA $\pi$ stacks. Int. J. Quantum Chem. *111*, 191–201.

59. Sevilla, M.D., Becker, D., Yan, M., and Summerfield, S.R. (1991). Relative abundances of primary ion radicals in .gamma.-irradiated DNA: cytosine vs. thymine anions and guanine vs. adenine cations. J. Phys. Chem. *95*, 3409–3415.

60. Schuster, G.B., and Landman, U. (2004). The mechanism of long-distance radical cation transport in duplex DNA: ion-gated hopping of polaron-like distortions. Top. Curr. Chem. *236*, 139–161.

61. Shukla, M.K., and Leszczynski, J. (2008). In Radiation Induced Molecular Phenomena in Nucleic Acid, M.K. Shukla and J. Leszczynski, eds. (Netherlands: Springer Science+Business Media).

62. Close, D.M. (2004). Calculation of the ionization potentials of the DNA bases in aqueous medium. J. Phys. Chem. A *108*, 10376–10379.

63. Pacheco-Ortín, S., Lozano, R.G., and Valdés, E.A. (2012). Possible DNA damage by oxidation products of guanine: a density functional and electron propagator theoretical study. Int. J. Quantum Chem. *112*, 2840–2847.

64. Gu, J., Xie, Y., and Schaefer, H.F., 3rd (2005). Structural and energetic characterization of a DNA nucleoside pair and its anion: deoxyriboadenosine (dA)-deoxyribothymidine (dT). J. Phys. Chem. B *109*, 13067–13075.

65. Lewis, F.D., Liu, J., Weigel, W., Rettig, W., Kurnikov, I.V., and Beratan, D.N. (2002). Donor-bridge-acceptor energetics determine the distance dependence of electron tunneling in DNA. Proc. Natl. Acad. Sci. USA *99*, 12536–12541.

66. Giese, B. (2000). Long-distance charge transport in DNA: the hopping mechanism. Acc. Chem. Res. *33*, 631–636.

67. Siriwong, K., and Voityuk, A.A. (2012). Electron transfer in DNA. WIREs Comput. Mol. Sci. *2*, 780–794.

68. Marcus, R.A. (1997). Electron transfer reactions in chemistry theory and experiment. J. Electroanal. Chem. *438*, 251–259.

69. Marcus, R.A., and Sutin, N. (1985). Electron transfers in chemistry and biology. Biochim. Biophys. Acta Rev. Bioenerg. *811*, 265–322.

70. Bolton, J.R., and Archer, M.D. (1991). Basic electron-transfer theory. In Electron Transfer in Inorganic, Organic, and Biological Systems, Volume 228, J.R. Bolton, N. Mataga, and G. McLendon, eds. (American Chemical Society), pp. 7–23.

71. Rösch, N., and Voityuk, A.A. (2004). Quantum chemical calculation of donor–acceptor coupling for charge transfer in DNA. In Long-Range Charge Transfer in DNA II, Volume 237, G.B. Schuster, ed. (Springer-Verlag Berlin Heidelberg), pp. 37–72.

72. Cave, R.J., Newton, M.D., Kumar, K., and Zimmt, M.B. (1995). Theoretical study of solvent effects on the electronic coupling matrix element in rigidly linked donor-acceptor system. J. Phys. Chem. *99*, 17501–17504.

73. Cave, R.J., and Newton, M.D. (1996). Generalization of the Mulliken-Hush treatment for the calculation of electron transfer matrix elements. Chem. Phys. Lett. *249*, 15–19.

74. Cohen, A.J., Mori-Sánchez, P., and Yang, W. (2008). Insights into current limitations of density functional theory. Science *321*, 792–794.

75. Dreuw, A., and Head-Gordon, M. (2005). Single-reference ab initio methods for the calculation of excited states of large molecules. Chem. Rev. *105*, 4009–4037.

76. Siriwong, K., Voityuk, A.A., Newton, M.D., and Rösch, N. (2003). Estimate of the reorganization energy for charge transfer in DNA. J. Phys. Chem. B *107*, 2595–2601.

77. Saito, I., Nakamura, T., Nakatani, K., Yoshioka, Y., Yamaguchi, K., and Sugiyama, H. (1998). Mapping of the hot spots for DNA damage by one-electron oxidation: efficacy of GG doublets and GGG triplets as a trap in long-range hole migration. J. Am. Chem. Soc. *120*, 12686–12687.

78. Steenken, S., and Jovanovic, S.V. (1997). How easily oxidizable is DNA? One-electron reduction potentials of adenosine and guanosine radicals in aqueous solution. J. Am. Chem. Soc. *119*, 617–618.

79. Voityuk, A.A. (2006). Computational modeling of charge transfer in DNA. In Computational Studies of RNA and DNA, J. Šponer and F. Lankaš, eds. (Springer, Dordrecht), pp. 485–511.

80. Senthilkumar, K., Grozema, F.C., Guerra, C.F., Bickelhaupt, F.M., and Siebbeles, L.D.A. (2003). Mapping the sites for selective oxidation of guanines in DNA. J. Am. Chem. Soc. *125*, 13658–13659.

81. Giese, B., Amaudrut, J., Köhler, A.K., Spormann, M., and Wessely, S. (2001). Direct observation of hole transfer through DNA by hopping between adenine bases and by tunnelling. Nature *412*, 318–320.

82. Kumpulainen, T., Lang, B., Rosspeintner, A., and Vauthey, E. (2017). Ultrafast Elementary Photochemical Processes of Organic Molecules in Liquid Solution. Chem. Rev. *117*, 10826–10939.

83. Takada, T., Kawai, K., Fujitsuka, M., and Majima, T. (2005). Contributions of the distance-dependent reorganization energy and proton-transfer to the hole-transfer process in DNA. Chemistry *11*, 3835–3842.

84. Voityuk, A.A. (2009). Can charge transfer in DNA significantly be modulated by varying the pi stack conformation? J. Phys. Chem. B *113*, 14365–14368.

85. Khan, A. (2008). Reorganization energy, activation energy, and mechanism of hole transfer process in DNA: a theoretical study. J. Chem. Phys. *128*, 075101–075106.

86. Voityuk, A.A. (2005). Are radical cation states delocalized over GG and GGG hole traps in DNA? J. Phys. Chem. B *109*, 10793–10796.

87. Frisch, M.J., Trucks, G.W., Schlegel, H.B., Scuseria, G.E., Robb, M.A., Cheeseman, J.R., Scalmani, G., Barone, V., Mennucci, B., Petersson, G.A., et al. (2009). Gaussian 09, Revision A.02 (Wallingford, CT: Gaussian).

88. Pérez, A., Luque, F.J., and Orozco, M. (2012). Frontiers in molecular dynamics simulations of DNA. Acc. Chem. Res. *45*, 196–205.

89. Garrec, J., Patel, C., Rothlisberger, U., and Dumont, E. (2012). Insights into intrastrand cross-link lesions of DNA from QM/MM molecular dynamics simulations. J. Am. Chem. Soc. *134*, 2111–2119.

90. Owczarzy, R. (2005). Melting temperatures of nucleic acids: discrepancies in analysis. Biophys. Chem. *117*, 207–215.

91. Tavernelli, I., Röhrig, U.F., and Rothlisberger, U. (2005). Molecular dynamics in electronically excited states using time-dependent density functional theory. Mol. Phys. *103*, 963–981.

92. Monari, A., Rivail, J.-L., and Assfeld, X. (2013). Theoretical modeling of large molecular systems. Advances in the local self consistent field method for mixed quantum mechanics/molecular mechanics calculations. Acc. Chem. Res. *46*, 596–603.

93. Lameira, J., Alves, C.N., Moliner, V., Martí, S., Castillo, R., and Tuñón, I. (2010). Quantum mechanical/molecular mechanical molecular dynamics simulation of wild-type and seven mutants of CpNagJ in complex with PUGNAc. J. Phys. Chem. B *114*, 7029–7036.

94. Brunk, E., and Rothlisberger, U. (2015). Mixed quantum mechanical/molecular mechanical molecular dynamics simulations of biological systems in ground and electronically excited states. Chem. Rev. *115*, 6217–6263.

95. Dans, P.D., Ivani, I., Hospital, A., Portella, G., González, C., and Orozco, M. (2017). How accurate are accurate force-fields for B-DNA? Nucleic Acids Res. *45*, 4217–4230.

96. Ivani, I., Dans, P.D., Noy, A., Pérez, A., Faustino, I., Hospital, A., Walther, J., Andrio, P., Goñi, R., Balaceanu, A., et al. (2016). Parmbsc1: a refined force field for DNA simulations. Nat. Methods *13*, 55–58.

97. Hypercube. (2007). HyperChem Professional, evaluation version 8 (Hypercube).

98. Allen, T.W., Andersen, O.S., and Roux, B. (2006). Ion permeation through a narrow channel: using gramicidin to ascertain all-atom molecular dynamics potential of mean force methodology and biomolecular force fields. Biophys. J. *90*, 3447–3468.

99. Cornell, W.D., Cieplak, P., Bayly, C.I., Gould, I.R., Merz, K.M., Ferguson, D.M., Spellmeyer, D.C., Fox, T., Caldwell, J.W., and Kollman, P.A. (1995). A second generation force field for the simulation of proteins, nucleic acids, and organic molecules. J. Am. Chem. Soc. *117*, 5179–5197.

100. Jorgensen, W.L., Chandrasekhar, J., and Madura, J.D. (1983). Comparison of simple potential functions for simulating liquid water. J. Chem. Phys. *79*, 926–935.

101. Hypercube. (2002). HyperChem release 8, tool for molecular modeling (Hypercube).

102. Lin, H., and Truhlar, D.G. (2007). QM/MM: What have we learned, where are we, and where do we go from here? Theor. Chem. Acc. *117*, 185–199.

103. Mayhall, N.J., and Raghavachari, K. (2010). Charge transfer across ONIOM QM:QM boundaries: the impact of model system preparation. J. Chem. Theory Comput. *6*, 3131–3136.

104. Dapprich, S., Komáromi, I., Byun, K.S., Morokuma, K., and Frisch, M.J. (1999). A new ONIOM implementation in Gaussian98. Part I. The calculation of energies, gradients, vibrational frequencies and electric field derivatives. J. Mol. Struct. Theochem *461–462*, 1–21.

105. Lin, H., and Truhlar, D.G. (2005). Redistributed charge and dipole schemes for combined quantum mechanical and molecular mechanical calculations. J. Phys. Chem. A *109*, 3991–4004.

106. Gu, J., Xie, Y., and Schaefer, H.F., 3rd (2006). Electron attachment to nucleotides in aqueous solution. ChemPhysChem *7*, 1885–1887.

107. Gu, J., Xie, Y., and Schaefer, H.F., 3rd (2007). Electron attachment to DNA single strands: gas phase and aqueous solution. Nucleic Acids Res. *35*, 5165–5172.

108. Gu, J., Wang, J., and Leszczynski, J. (2010). Electron attachment-induced DNA single-strand breaks at the pyrimidine sites. Nucleic Acids Res. *38*, 5280–5290.

109. Hehre, W.J., Radom, L., Schleyer, P., and Pople, R.J.A. (1986). Ab Initio Molecular Orbital Theory (New York: Wiley), pp. 63–101.

110. Rugne, E., and Gross, E.K.U. (1984). Density-Functional Theory for Time-Dependent Systems. Phys. Rev. Lett. *52*, 997–1000.

111. Miertus, S., and Tomasi, J. (1982). Approximate evaluations of the electrostatic free energy and internal energy changes in solution processes. Chem. Phys. *65*, 239–245.

112. Marenich, A.V., Jerome, S.V., Cramer, C.J., and Truhlar, D.G. (2012). Charge Model 5: An Extension of Hirshfeld Population Analysis for the Accurate Description of Molecular Interactions in Gaseous and Condensed Phases. J. Chem. Theory Comput. *8*, 527–541.

113. Accelrys Software. (2005). Accelrys DS Visualizer v.2.0.1.7347 computer program, freeware version (Accelrys Software).

114. Zheng, G., Lu, X.J., and Olson, W.K. (2009). Web 3DNA–a web server for the analysis, reconstruction, and visualization of three-dimensional nucleic-acid structures. Nucleic Acids Res. *37*, W240–W246.